POLITECNICO DI TORINO

Master's Degree in
Nanotechnologies for ICTs

Master's Degree Thesis

Controlling magnetic skyrmion Brownian motion through Focused-Ion-Beam patterning

Supervisors	Candidate
Prof. Fabrizio Riente	**Donatella Albano** 306048
Prof. Markus Becherer	
Dr. Valentin Ahrens	

Academic Year 2024-2025

Controlling magnetic skyrmion Brownian motion through Focused-Ion-Beam patterning

Donatella Albano

Summary

Today the scaling down of physical dimensions in CMOS devices is reaching its end, and lots of research is devoted to explore other possibilities to perform computation and memory functions. Magnetic devices enter in the beyond-CMOS field as they offer the advantages of non-volatility and low power operation for logic functions. This thesis focuses on magnetic skyrmions, which are particle-like topological spin textures, nucleated by magnetic fields in thin films of magnetic materials. The interface properties of the magnetic stack are modified with ion implantation through Focused-Ion-Beam, with the intent of creating nucleation sites and tracks for skyrmions, where they are moved through current. In FIB irradiated states, skyrmions exhibit Brownian motion; indeed they are fluctuating and the random motion is affected by the ion dose. In this thesis it is investigated the effect of ion implantation on diffusion.
Fluctuations are essential for biological functions and exploiting the "richness" of diffusion can be beneficial in a skyrmion device. Unconventional computing paradigms present a good example of applications in which Brownian motion can be harnessed. The future use of skyrmion diffusion is directly linked to this kind of applications and the goal of this work is to find a way to modulate diffusion through ion implantation.

The study of skyrmions moving with Brownian motion is carried on sputtered W/CoFeB/MgO/Ta thin film, where $80 \times 80\,\mu m^2$ squares are irradiated with Gallium ions. The ion doses vary from 1×10^{12} ions/cm^2 to 1×10^{13} ions/cm^2 and the outcome of irradiation is observed with a Widefield-MOKE microscope, as visualized in Fig 1.

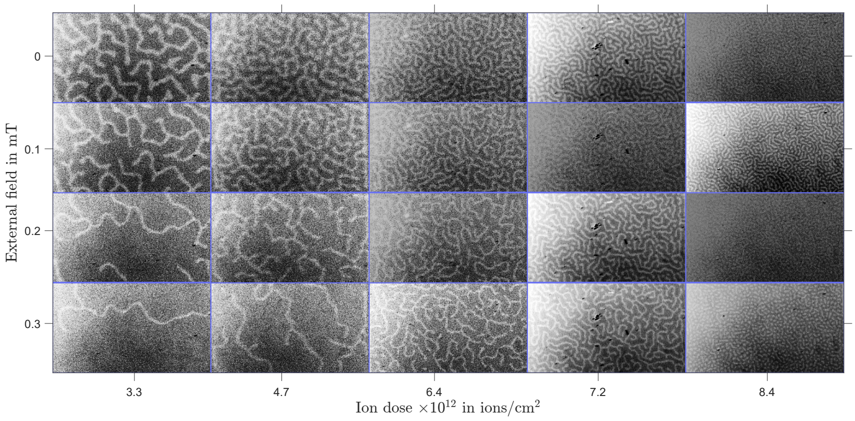

Figure 1: Magnetic phase diagram of domain structures in Ga-ion-irradiated portions in the sample.

Magnetic domains become smaller with higher magnetic fields, and this trend is enhanced for higher ion doses. Indeed, for higher fluences domains shrink till

skyrmions appear and skyrmions in those irradiated states can be nucleated at lower magnetic fields.

The next step of the study has been the investigation of Brownian motion and the analysis of its dependence on the ion dose. Skyrmion motion is recorded through the PCO camera on the WMOKE microscope and the obtained videos are collection of frames take 0.05 seconds apart. These videos are processed with Fiji, an image processing package of ImageJ and then skyrmions are detected and their positions connected exploiting TrackMate, the tracking tool provided by Fiji. In this way skyrmion trajectories are ready to be analyzed. The information on the kind of motion and diffusivity are extracted from the trajectories thanks to the MSDanalyzer, which is a Matlab class specialized to perform the Mean Square Displacement (MSD) analysis. The latter is a widely used technique in colloidal science and biophysics to identify the mode of motion of particles tracked over time. If the MSD follows a linear trend, the particle is undergoing diffusion, and the slope of the line corresponds to the diffusion coefficient.

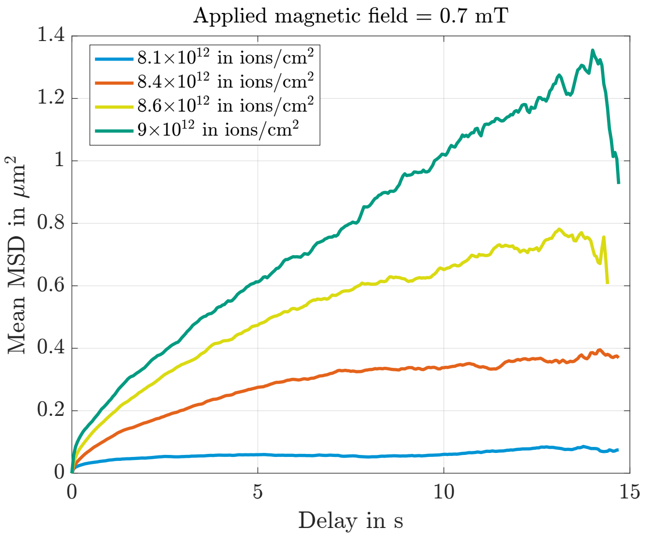

Figure 2: Analysis of skyrmion diffusivity for ion doses from 8.1×10^{12} ions/cm^2 to 9×10^{12} ions/cm^2 at 0.7 mT.

The plots in Fig 2 reveal an increase of the linear trend for higher ion doses. While the MSD saturates and has a concave curvature for lower ion doses, which implies that the skyrmion movement is impeded. Confined motion arises due to pinning centers that act as traps for skyrmions. Ion irradiation increases the intermixing between atoms at the interface of the magnetic stack, and this causes the reduction of pinning. Hence, through ion irradiation, skyrmion diffusion can be enhanced.

The idea is to exploit Brownian motion to obtain directed motion by creating a gradient of ion doses with FIB. The gradient is engineered to force skyrmions to diffuse from low to high ion doses.

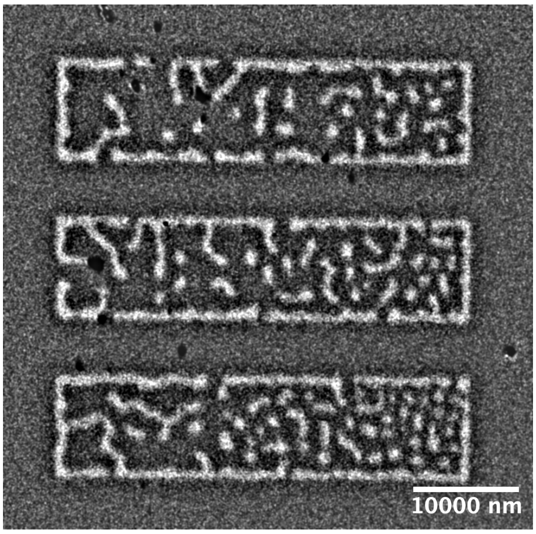

Figure 3: WMOKE image at 0.7 mT of three rectangles patterned with gradients of ion doses.

To achieve this goal, not only are gradients patterned, but the pattern is shaped as a rectangle to favor the directionality of motion, as visualized in Fig 3. Also, the density of skyrmions is modulated with the gradient, and this is clear by observing Fig 3 and the squares with skyrmions in Fig 1. Analyzing skyrmion trajectories in gradients, directionality is not achieved. However, the diffusivity is higher than in the case with a single ion dose. The enhancement of diffusivity that happens within gradients can be exploited in devices that rely on diffusion, like the reshuffler used for stochastic computing. In the latter case, increasing the diffusivity positively impacts the computational time.

This first attempt to tune the skyrmion Brownian motion through Gallium ions is the starting point for future studies. It has shown the versatility of diffusion and how the latter adds another layer of complexity to magnetic skyrmions, and if leveraged, diffusion opens new functionalities for skyrmion devices.

ACKNOWLEDGMENTS

Firstly, I would like to thank the Politecnico of Turin and Prof. Fabrizio Riente for allowing me to work on the thesis abroad.

I also want to say a big thank you to Prof. Markus Becherer for welcoming me into the Nanomagnetic Devices group at the Technical University of Munich (TUM).

There, I was introduced to this fascinating topic by Dr. Valentin Ahrens. I appreciated his guidance, and I am grateful for this first glimpse at research that has inspired me for this study, and I will cherish it in the future.

Table of Contents

List of Figures

List of Tables

Chapter 1

Introduction

1.1 Emerging technologies beyond Moore's law

Since the 1960s Moore's law has dominated the information technology industry. It states that the number of transistors on a microprocessor chip doubles every two years. Together with the density of transistors, the performance has improved as well, and the main driving force has been the scaling down of the circuit elements. To make sure that the right upgrades were made, the semiconductor industry has been coordinated through a research road map. In this way, what was an empirical law actually became true and the industry itself reinforced this mechanism.

Today, the idea of scaling down poses many problems, such as leaking currents, quantum effects, and heat dissipation, and the search for alternatives has begun. Together with new physical mechanisms, there is a shift from the traditional computing models to new ones like "in-memory computing", which performs fundamental logical operations within the memory.

A possible realization is offered by skyrmion-based spintronics. Spintronics is a field based on the interaction between the spin degree of freedom of an electric current with a magnetic material. Specifically, this thesis harnesses magnetic skyrmions, which are spin textures, as magnetic bits in memory and computing devices. In 1961 the concept of skyrmions was proposed by Tony Skyrme in a model describing localized field configurations that behave like particles. Then this idea spread far beyond nuclear physics and has been applied in a wide variety of systems. Their theoretically existence in magnetic systems was predicted in 1989, and was experimentally observed in 2009, thanks to neutron scattering experiments that revealed a 2D hexagonal skyrmion lattice in the MnSi chiral magnet. Later, magnetic skyrmions have been demonstrated in thin films with heavy metals interfaces.

Today, these magnetic textures are attracting progressively more attention in the scientific community.

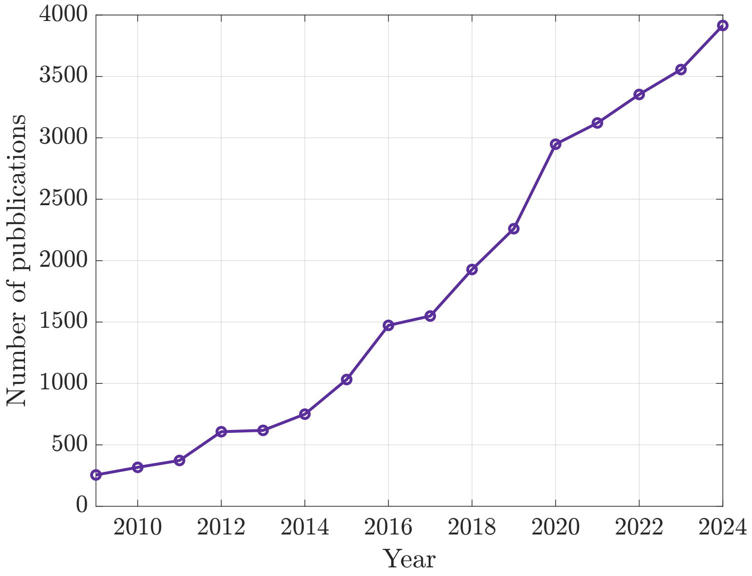

Figure 1.1: Yearly number of published papers related to skyrmions, since their experimental observation in 2009.

The attention towards magnetic skyrmions is owed to several advantages that they offer, such as low driving currents, nanoscale size, and non-volatility. Moreover, their motion can be efficiently tuned to achieve high-speed operation. However, their dynamics are complex and engineering skyrmions for transistor-like devices, pose some challenges due to their thermal fluctuations and interactions with defects in the magnetic thin films. Instead of overcoming the problems posed by these properties, there is the opportunity to take advantage of them in unconventional computing applications [1].

1.2 Magnetism

Magnetic skyrmions are hosted in thin-film systems with magnetic behavior. In order to understand their origin, their characteristics and how they can be manipulated, first a description of magnetism at the atomic level is necessary.

1.2.1 Magnetic interactions

A magnetic system consists of electrically charged particles with an angular moment and a magnetic moment originating from their spin and their orbital angular momentum. Magnetic phenomena can be classified depending on the kind of alignment between magnetic moments. If adjacent magnetic moments are aligned parallel to one another, the magnetic ordered state is ferromagnetic. The positioning of the magnetic moments is a complex processes, determined by the interplay of energies able to arrange atomic spins; here, the focus is on the most relevant interactions for magnetic skyrmions.

- The **exchange interaction** occurs between identical particles, it is a quantum-mechanical effect that happens due to the overlapping wavefunctions of neighboring atoms. It leads to the alignment of atomic spins with respect to each other.

- The **Dzyaloshinskii-Moriya interaction** (DMI), is a chiral interaction coming from the lack or from the breaking of inversion symmetry. Its effect is the canting of neighboring spins. This kind of interaction can be found in bulk materials that present high spin orbit coupling (bulk DMI) or in thin films at the interface between a heavy metal with large spin-orbit coupling and a ferromagnetic material (interface DMI) [2]. In the latter case, it is the presence of different atoms at the interface that creates this kind of interaction, as it is visualized in Fig 1.2.

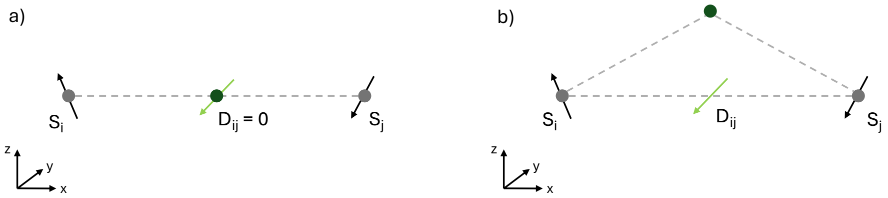

Figure 1.2: Sketch of the Dzyaloshinskii-Moriya interaction. (a) The inversion symmetry is not broken, so there is no DMI. (b) The green atom is no longer in between the two atoms with spin, the inversion symmetry is broken, thus there the DMI is not null.

- The anisotropy energy is a kind of energy that sets the favorable directions (easy-axes) for magnetization, which is the magnetic moment per unit volume. For example, the **magnetocrystalline anisotropy** arises thanks to the symmetry of atomic spins in the hosting lattice. While the presence of an interface, as it is in thin films, supports the **interface anisotropy**, which adds up to the anisotropy energy.
- The **Zeeman energy** refers to the external field energy, given by the interplay between the magnetization and the external magnetic field. This energy favors the alignment along the field.
- When a body is uniformly magnetized, at any internal or external surfaces, there are discontinuities in the magnetization. The latter are explained as if there are "free poles", that are not balanced by poles of opposite kind in the vicinity. So, they create a field, the **demagnetizing field** that has the opposite direction with respect to the magnetization. This kind of magnetic field has its own energy term, the **magnetostatic energy**.

1.2.2 Magnetic domains

By observing a magnetic body at the microscale, the magnetic texture shows sub-regions with uniform magnetization. The latter are called magnetic domains. The

concept of magnetostatic energy explains their formation.
In the absence of an applied field, the magnetostatic energy depends on the demagnetizing field and if the single domain is split in more domains, the poles disappear and the demagnetizing field is minimized, as visualized in Fig 1.3.

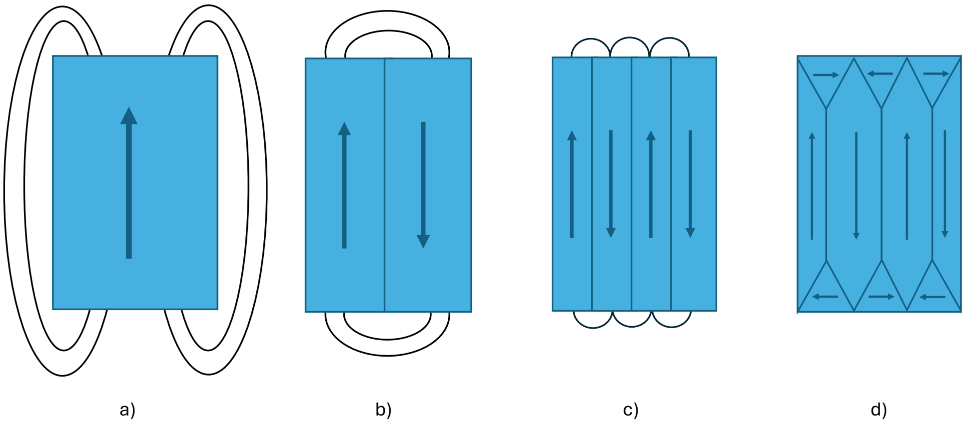

Figure 1.3: Visualization of the division into domains to reduce the magnetostatic energy. a) The magnetization is along one direction and the magnetostatic energy is large; the reduction of the magnetostatic energy happens when there is the splitting b) into two domains and c) into four domains, and d) closure domains minimize the magnetostatic energy.

Anytime there is a change in the conditions, for example if an external magnetic field is present, the domain structure rearranges itself as to balance all the magnetic interactions. For low magnetic fields, the domains with the magnetization oriented parallel to the field are enlarged, while those oriented antiparallel shrink. Increasing the magnetic field when the saturation magnetization is reached, all opposite magnetized domains disappear. Measuring the samples magnetization while cycling results in a hysteresis loop, where the magnetization has different values depending on whether the magnetic field is increasing or decreasing. This non-linear response to an external field is typical of ferromagnets.

1.2.3 Domain walls

The change of the magnetization's direction between two domains is not discontinuous, it happens in a transition region, called the domain wall, where magnetic moments rotate. The trend of increasing the number of domains by decreasing the magnetostatic energy is limited by the presence of domain walls, because with the creation of a domain wall the exchange energy as well as the anisotropy are increasing, and app up to the energy balance [3]. This further justifies the idea for which all magnetic interactions influence the achievement of the equilibrium structure, till reaching the minimum energy configuration.
There are two types of domain walls, that differentiate from one another in the way the atomic magnetic moments turn in the wall (Fig 1.4).

- Bloch domain wall: where the magnetic moments turn in a plane perpendicular to the line connecting two domains.
- Néel domain wall: where the moments in the wall are confined to the same plane of the moments in the domain.

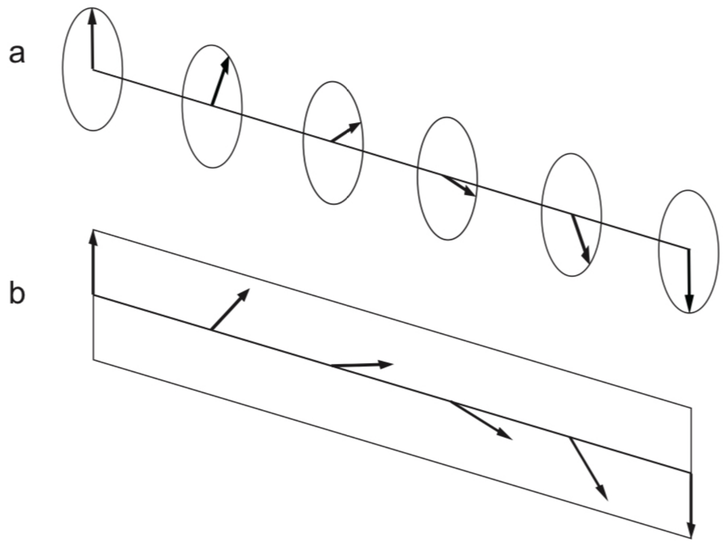

Figure 1.4: Types of domain walls: (a) Bloch wall and (b) Néel wall [3].

1.3 Magnetic skyrmions

Magnetic skyrmions are topological swirling spin configurations that exhibit unique quasi-particle properties. As for domains, they are formed as a result of a competition between different forces. The main interaction that allows skyrmion stabilization in ferromagnetic systems is the DMI. The DMI makes adjacent magnetic spins to have a preferential fixed angle between each other and the spin direction gradually changes from the outer edge to the center, showing chirality. Generally there are two types of magnetic skyrmions (Fig 1.5), that differentiate one from another for the way that spins rotate and emerge from two different physical mechanisms.

- Néel-type skyrmion: the spins rotate in the radial planes from the core to the outer edge. They are supported by interfacial DMI, so they are typical of thin-films.
- Bloch-type skyrmion: the magnetic moments rotate in the tangential plane, that is, perpendicular to the radial directions, when moving from the core to the outer edge. They can be found in bulks of ferromagnets, due to the presence of bulk DMI.

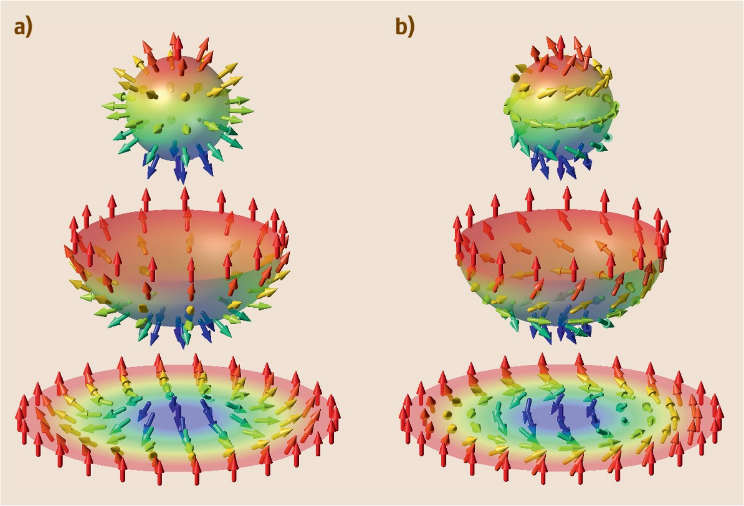

Figure 1.5: Schematic picture of (a) Néel skyrmion and its mapping onto a sphere (hedgehog configuration), (b) Bloch skyrmion (combed hedgehog configuration) [4].

What makes skyrmions unique is their topology and they are described by a topological charge, which quantifies the "winding" of the magnetic spins of a skyrmion. A topological feature is a characteristic of an object that remains unchanged under continuous deformations, so the topological charge is a conserved quantity. Thus, this characteristic is responsible for skyrmions increased stability, which is one of their proprieties attracting research interest. The topological charge, or skyrmion number, counts how many times the magnetic texture wraps a unit sphere. It can be calculated based on the exact spin texture configuration according to the following analytical formula

$$Q = \frac{1}{4\pi} \int d^2\mathbf{r} \cdot \mathbf{m}(\mathbf{r}) \cdot (\partial_x \mathbf{m}(\mathbf{r}) \times \partial_y \mathbf{m}(\mathbf{r})) \tag{1.1}$$

where $\mathbf{m}(\mathbf{r})$ is the local magnetization. The skyrmions can be mapped to a sphere, putting the spin of the core at the south pole, the spins at the boundary at the north pole, and projecting all the other spins in between around the sphere. The direction of the magnetization in the core of the skyrmion is called polarity. For both Bloch and Néel type of skyrmions, when the polarity is pointing down and at the boundary the spins are pointing up, the skyrmion number is $Q = -1$, since the twisting of spins is negatively oriented. However, there are more possibilities for spin textures arrangements, and some others, such as the antiskyrmion or the bimeron, have $Q = -1$ as well. It is out of the scope of this thesis to describe these kind of spin textures, but highlighting this shared feature poses the need for more figures of merit. Thus, the topological spin texture is fully characterized by three distinct numbers (Q, Q_v, Q_h) [5]. The vorticity number Q_v for skyrmions describes the in-plane spin texture. While, the helicity number Q_h is determined from the type of DMI that stabilizes the skyrmion, for Bloch skyrmions it could be $\pi/2$ or $3\pi/2$ and for Néel skyrmions either 0 or π.

1.3.1 Skyrmion dynamics

The skyrmions capacity to be efficiently manipulated even with ultra-low current densities makes them excellent candidates for logic based spintronic devices. Moreover, in thin films the integration of skyrmions intrinsic 2D nature enables for device geometries that could be potentially more efficient than 1D tracks required for domain wall motion.

When subjected to a current, in materials with strong spin-orbit coupling, like heavy metals, occurs the Spin Hall Effect (SHE). It generates a transverse spin current, since the current flow causes electrons with opposite spins to be deflected in opposite directions. The movement of skyrmions by an electronic current is mainly controlled by two mechanisms.

- Spin-Transfer Torques (STT): this effect occurs when a spin-polarized current flows through a ferromagnetic layer. The electrons in the spin-polarized current tend to align their spin with the magnetic material magnetization. As the spin orientation of an electron is changed, the angular momentum is conserved and this results in a torque that modifies the local magnetic configuration. This affects the domain wall at the boundary of a skyrmion, causing it to push skyrmions.

- Spin-Orbit Torques (SOT): this other mechanism works only in systems with a heavy metal and adjacent to the ferromagnetic layer. Due to the Spin Hall Effect, a current applied in the heavy metal generates a transverse spin current. This spin current extends to the adjacent ferromagnet and produces a torque on the magnetic structure. As for the STT, this torque moves domain walls and consequently skyrmions.

1.3.2 Magnetic stack

The magnetic properties that arise in nanometric systems arise thanks to the broken translational symmetry of the atoms that compose these systems. This happens when magnetic moments experience different neighbors in their vicinity, thus at the interface. Indeed, the system under study exploits interface effects in a stack of different layers at the nanometric scale. Sputtered thin films made up of a heavy metal layer, a magnetic layer and another heavy metal layer or an oxide have proved to be optimal systems to host skyrmions. The magnetic stack chosen for this skyrmion study is $W_{(3)}/CoFeB_{(1)}/MgO_{(1)}/Ta_{(3)}$, the thicknesses of the layers are expressed in nm in the subscripts.

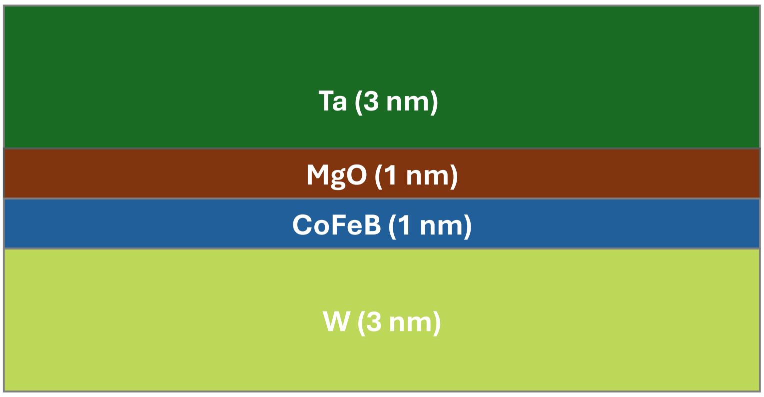

Figure 1.6: Illustration of the magnetic thin film stack employed in this study.

The materials in the stack are selected to have strong perpendicular magnetic anisotropy (PMA), which means that the easy axis is in the direction perpendicular to the surface. PMA arises at the ferromagnet-oxide interface, as for CoFeB/MgO, due to the hybridization between the oxygen and the magnetic transition metal orbits across the interface. Furthermore, to obtain strong DMI the seed layer made of W is needed, because this metal shows high spin-orbit coupling, while the capping layer is made of Ta.

1.3.3 Nucleating skyrmions in ion-irradiated states

One critical step for developing skyrmion-based devices is the nucleation of skyrmions. The established nucleation methods are based on: electrical currents, laser pulses, and electrical fields. Focused-Ion-Beam (FIB) irradiation offers the possibility to finely tuning the magnetic properties of the system, with the effect of modifying the magnetic field at which skyrmions nucleate. Ions are shot with high precision in a defined region of the sample and they modify the crystalline structure of the film, changing the magnetic properties. This technique enables nanometer-scale manipulation of magnetic media. Moreover, the chosen magnetic stack is compatible with CMOS technology and FIB is widely employed in the semiconductor industry for subtractive processes [6], making this skyrmion-base system highly promising for integration with existing technology and more convenient to be fabricated. Moreover, as it is pointed out in [7], ion implantation can easily modulate magnetic properties without etching, so introducing less defects.
When light ions like He+ travel in the material stack, they induce short-range atomic displacements that lead to interface intermixing and alter interface driven properties, like PMA and DMI. Increasing the irradiation fluence results in a reduction of PMA. Using heavier elements, as Ga ions, the effects of irradiation are different [8]. Investigating the usage of Ga+ in Ta/CoFeB/MgO thin films, showed intermixing at the Ta/CoFeB interface and this could be the reason for a decrease in the saturation magnetization and the increase of DMI. Meanwhile, the accumulation of Ta at the CoFeB/MgO interface could explain the reduction of anisotropy. Intermixing has

been observed in a stack with a different seed layer, W in place of Ta. In the irradiated part of the sample, larger domains appear and carefully choosing the applied magnetic field they are shrinked and then compressed into skyrmions. With the application of a current is possible to observe that skyrmions are moving as rigid objects and their typical transverse motion, due to the Skyrmion Hall Effect (SkHE) that arises from the topological nature of skyrmions [9]. The SkHE makes the skyrmion to move at an angle with respect to the applied driving force and this affects the direction of current driven skyrmions, eventually leading to their annihilation due to interactions with the sample boundaries.

1.3.4 Tuning skyrmion density

The study of the magnetic structure is carried out with the home-built wide-field magneto-optical Kerr effect (WMOKE) microscope (see appendix A.2).

On the thin film a series of $80 \times 80\,\mu m^2$ squares is irradiated with ion doses in a range from $1 \times 10^{12}\,ions/cm^2$ to $1 \times 10^{13}\,ions/cm^2$ with Focused Ion Beam (see appendix A.1). An ion dose is a term to define the impacted quantities of ions onto the substrate through an area. In this magnetic stack before ion irradiation, skyrmions were not obtained by field cycling. To each square corresponds a different ion dose and the images with the WMOKE show the effect of Ga+ irradiation on the magnetic layers.

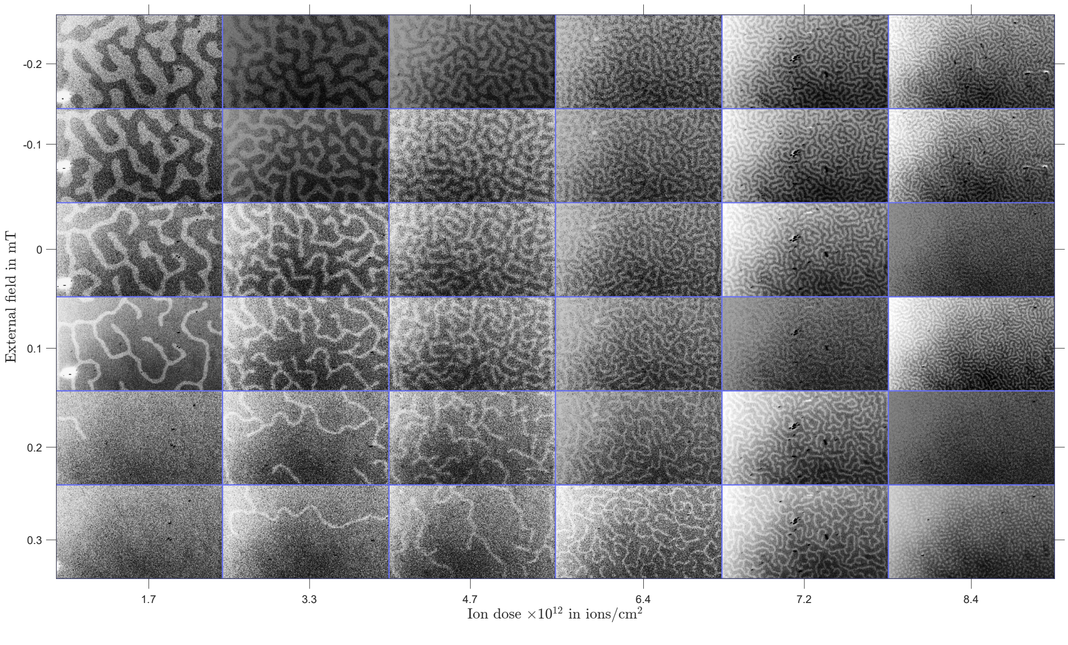

Figure 1.7: Magnetic phase diagram of domain structures in Ga-ion-irradiated portions in the sample. Each row shows squares with different ion dosages and at the same magnetic field. On the columns it is possible to look at the evolution of domains with the same ion dose and at different magnetic fields. An ion beam current of 7.7 pA and accelerating voltage of 30 keV have been used in the FIB settings.

The domains structure evolves with the magnetic field, as shown in Fig 1.7. For low ion dosages (from 1×10^{12} to 5×10^{12} ions cm^{-2}), the domains shrink with higher magnetic fields, but there are no skyrmions. While, increasing the ion dose the domains size reduces even more and for 7×10^{12} ions cm^{-2} domains start to rip apart and skyrmions appear mixed together with domains. Finally, for 8×10^{12} ions cm^{-2} and at 0.2 mT and 0.3 mT, the entire irradiated square is filled with skyrmions. Here, it is visible how the skyrmion density can be sharply increased with a slight increase of ion irradiation. The disorder introduced by Ga+ induces a decrease in the nucleation energy barrier of skyrmions. Structural disorder modifies local magnetic interactions, implying that less energy is needed to twist the spins into the skyrmion configuration in those regions, effectively lowering the energy cost of nucleation. Therefore, the magnetic field required to stabilize skyrmions in the breaking process decreases with the increase in the irradiation dose [10]. The outcome is that the ion dosage serves to tune the amount of structural changes in the magnetic layers and thus the skyrmion density, which has a profound effect on the skyrmions mobility. The evolution of domains has also been studied for higher ion dosages, but in that case, no domain patterns could be observed.

In previous studies, exploring the opportunity of tuning the velocity and the angle of current-driven skyrmions by high dose irradiation in W/CoFeB/MgO thin films, led to the observation of skyrmion Brownian motion [11]. This is a diffusive motion that can be detrimental for skyrmion applications. For example, if a skyrmion serves as an information carrier in a memory device, it must be locked in a specific location, and its Brownian motion can cause the displacement, hence the memory loss. Moreover, when skyrmions are directed by a current, Brownian motion affects the direction of motion and distorts the velocity.

Also in VLSI systems, noise and fluctuations compromise the reliability and today suppressing those is becoming more difficult. One of the proposed solutions is to exploit noise in circuits and use a random search to drive computation. The same idea can be beneficial for circuits that use magnetic skyrmions, for example tuning the Brownian motion for probabilistic computing purposes. Thus, it could be intriguing to look into the Brownian motion of skyrmions in ion irradiated systems and the possibility to exploit it for unconventional computing purposes.

1.4 Unconventional computing

The memory bottleneck of Von Neumann computing leads the search for unconventional computing architectures that process data more efficiently. Those computational schemes exploit behavioral phenomena occurring naturally in complex dynamical systems. Magnetic skyrmions possess a complex dynamics and rather than trying to fit them in already existing technologies like racetrack memories and logic gates, it would be beneficial to harness this complexity. Brownian motion makes skyrmion dynamics unique and it has been demonstrated that it is advantageous in several unconventional computing schemes.

1.4.1 Stochastic computing

Stochastic computing deals with probabilities instead of binary numbers. This probability is the number of times a 1 or a 0 appears in a random sequence of binary units. The probability values can be used in standard logic operations, with the advantage of low-energy cost implementations at the cost of less computational precision. An example of the multiplication operation is depicted in Fig 1.8a. Within the same example there is also illustrated the main limitation of stochastic computing, signal correlation (Fig 1.8b). Feeding two identical inputs produces an output that is not the product of the two signals. In stochastic computing to achieve a correct logical operation, there must be a mechanism for signal decorrelation. The element that allows to produce an uncorrelated copy of a signal with the same probability value is called a stochastic reshuffler (Fig 1.8c).

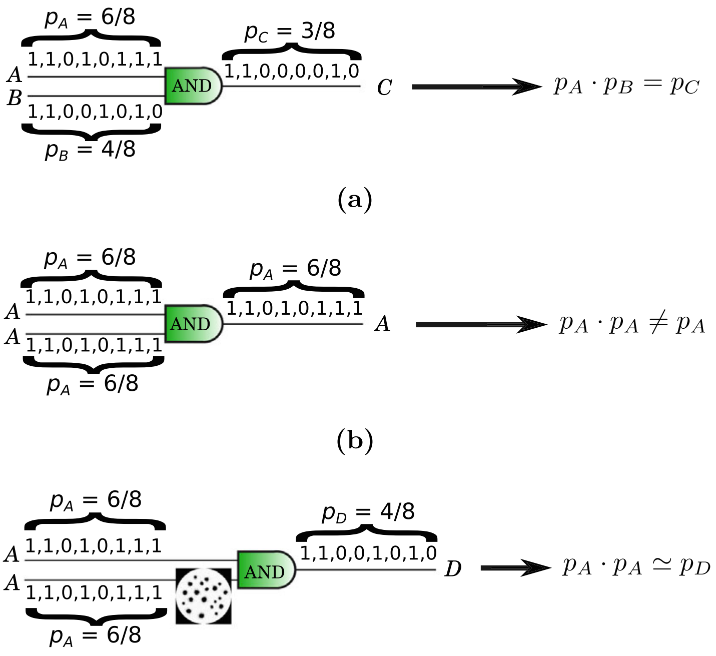

(a)

(b)

(c)

Figure 1.8: AND-gate implementation of the multiplication operation under the stochastic computing paradigm [12].

The idea of realizing a skyrmion reshuffler has been proposed in [12]. This device converts an input bit stream into a sequence of skyrmions whose order is reshuffled thanks to skyrmion diffusion. There are two chambers, each with input and output channels. Skyrmions out of the up chamber are read in the output signal as 1, while skyrmions from the down chamber are read in output as 0. In the chambers the skyrmions can diffuse, in this way the exiting order of 1 and 0 becomes random and the probability remains the same, since it depends only on the number of skyrmions in the system. Skyrmions are driven in the chambers by current and the decorrelation power of this device is inversely proportional to the time of reshuffling, hence the amount of current used. The experimental demonstration of this device with thermally diffusive skyrmions has been achieved in [13].

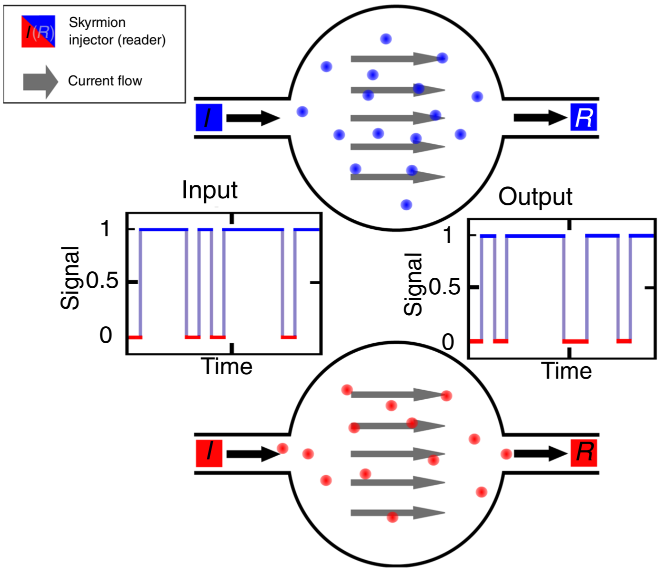

Figure 1.9: Skyrmion reshuffler device concept proposed by [12].

1.4.2 Neuromorphic computing

Neuromorphic computing emulates the physical nature of the human brain, designing devices with the same capabilities of synapses and neurons. A synapse acts as a switching medium to pass an electrical or chemical signal from one neuron to another. Skyrmion-based artificial synapse mimics the potentiation/depression process of a biological synapse for example by taking advantage of the current-driven motion of skyrmions.

A biological neuron can be divided into three functionally distinct parts, called dendrites, soma and axon. The dendrites collect signals from other neurons and transmit them to the soma. The latter processes the signal through a non-linear step. Finally, the axon takes the output signal and delivers it to other neurons. Neuronal dynamics are based on the registration of an input signal with a voltage increase and a mechanism that generates an output when a certain threshold voltage is triggered. However, in between incoming signals and before the threshold is reached, the neuron's voltage decays towards its resting potential. Therefore, the neuronal activity is described with the so-called "Leaky Integrate and Fire" (LIF) model.

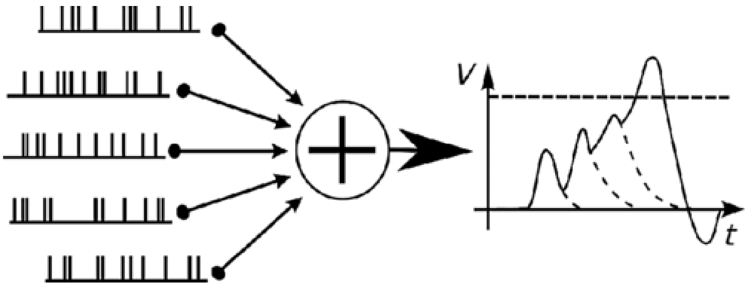

Figure 1.10: Schematic representation of how a neuron collects neuronal spiking activity from nearby neurons [12].

An artificial neuron can be designed according to the LIF model, having its typical three functionalities: integration, leaking, and firing. In the skyrmion-based artificial neuron, proposed in [12], they employed the same concept of a chamber with input and output channels of the reshuffler. This time, there is a voltage gate at which skyrmions accumulate before exiting the device. The neuron fires when a critical skyrmion density is achieved and the gate voltage is switched. Skyrmion diffusion is responsible for the "leaking". Within the same framework, both the neuron and the reshuffler exploit skyrmions Brownian motion, and it is evident how resourceful the diffusive behavior of skyrmions can be. Moreover, the characteristic feature of neurons, leaking, has also been obtained by leveraging the other competing forces typical of magnetic skyrmions [1].

1.4.3 Reservoir computing

A Recurrent Neural Network (RNN) has a similar structure to the human brain. Indeed, it is a network of nonlinear processing units (as neurons in the brain) with weighted connections between them (as the synapses) characterized by a flow of information in feedback loops. The latter is its main advantage but it is also the main limitation because training such complex network is computationally expensive. Reservoir Computing (RC) solves this issue because it trains only the output weights. The goal of RC is not to solve a complex problem, but to map it into a linearly solvable one. To do so, the reservoir projects different spatial-temporal events into a sparsely populated high dimensional space, where they become easier to recognize and categorize (Fig 1.11). Indeed, RC is suited for applications that involve recognition and classification of spatial-temporal events, like speech recognition or sensor fusion type applications. The requirements for a system to be the reservoir are non-linear response to input and previous state, and short term memory as to allow temporal input correlations.

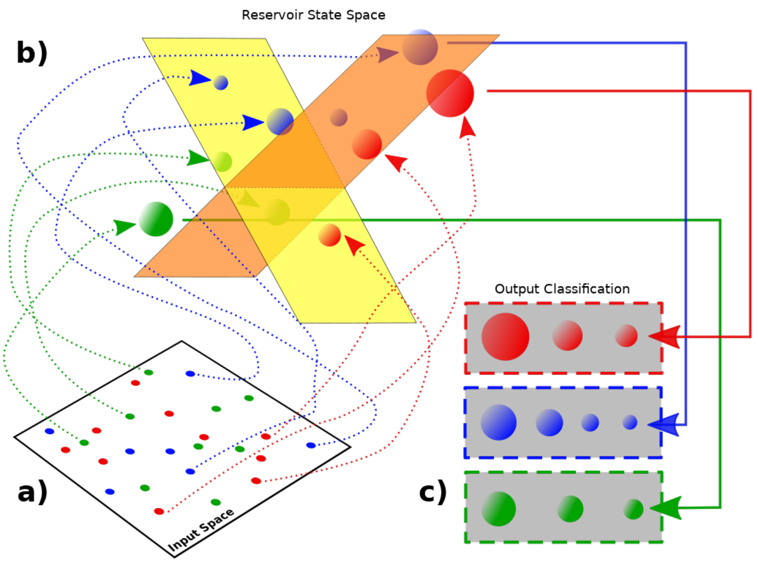

Figure 1.11: Schematic of the RC operational principle. (a) Unstructured data from an input space is (b) nonlinearly projected by the reservoir's transient dynamics onto its higher dimensional state space. Due to the similar evolution of the reservoir when driven similarly correlated input data samples (represented by similar colors), (c) a single linear regression step can be used to define hyperplanes in the reservoir's state space such that different data categories become separated [14].

An example of a RC component is realized in [15], exploiting geometrically confined skyrmions that are diffusing with Brownian motion. In this device the states of the system are the skyrmion positions, which result from the interplay of current induced motion due to SOT, the skyrmion edge repulsion and thermal diffusive dynamics, as it is visualized in Fig 1.12. The advantage of exploiting diffusion resides in the possibility to operate at low current densities.
These study cases open the path to more applications of Brownian motion in the context of unconventional computing, since each of them exploits the skyrmion fluctuations in a different way, and this underlines the versatility of diffusion, especially since it is driven at room temperature and is already embedded in magnetic skyrmions.

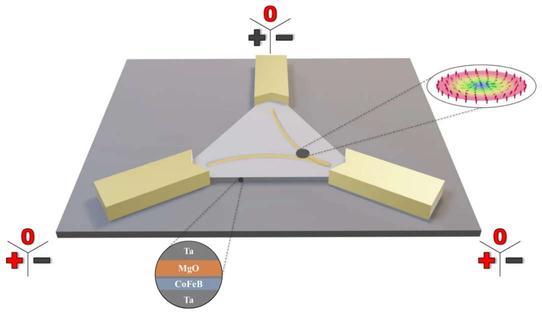

Figure 1.12: Three-dimensional schematic of the device. The dark gray spot in the triangle represents a skyrmion. It is pushed into the lower right corner [15].

Chapter 2

Brownian motion of magnetic skyrmions

2.1 Brownian motion

Brownian motion is a process strongly related to biology, indeed its name comes from the botanist Robert Brown. In the late 1820's, Brown observed under a microscope pollen grains suspended in water and noted that pollen grains ejected minute particles with erratic motion.

At the end of the century, Léon Gouy proposed that this perpetual motion is caused by thermal motion of the solvent molecules. Diffusion was an already known process, but only years later Einstein discovered the link between diffusion and Brownian motion. In his 1905 paper, Einstein stated that particles immersed in an ambient medium experience chaotic collisions with its molecules, that in turn cause their perpetual irregular motion. Einstein proposed a probabilistic derivation of the diffusion equation, based on the random walk model. From this framework come the equations necessary to analyze the Brownian motion of skyrmions.

Indeed, even though in the original context the medium is a fluid and the particle are in the micrometer range, the fluctuations in systems with nanometer scale features are described by Brownian motion as well.

2.2 Theory of the Mean Square Displacement

A random walk is a process by which objects move randomly and wander away from where they started. It is more common that objects experience a random walk in 2D or 3D systems, however to better understand this process, we start in a 1D system. At each movement step, the object has equal probability of moving forward or backward. After N steps, since the two displacements are equally likely to happen, the average displacement of the object would be zero. Nonetheless, to know how far the object moved in total, instead of the average traveled distance, the average of the square of the distance is employed, because it can't be averaged to zero. Consequently, the average of the square of the distance is equal to the number of steps, N.

Now, knowing that the mean square displacement (MSD) encodes the description of the random walk, we continue the analysis with a 2D system, which is also our case of interest. In a system with diffusing objects, whose positions are recorded in time, the MSD is the ensemble average of the time average of the single object MSD. The latter is calculated as

$$\mathrm{MSD}_i(\tau) = \sum_t \left(r_i(t+\tau) - r_i(t)\right)^2 \tag{2.1}$$

r_i is the position of the particle, and τ is called the delay, which spans from the smallest time difference between two positions to the total time of the random walk. This quantity expresses how long is the distance covered by that object with Brownian motion in a time τ. For the whole ensemble the MSD is

$$\mathrm{MSD}(\tau) = \frac{1}{N}\sum_{i=1}^{N} \mathrm{MSD}_i(\tau) \tag{2.2}$$

which highlights that the MSD, being an average, depends on the number N of objects in the system. According to Einstein theory for an ensemble of objects (particles) undergoing Brownian motion, the expression of the MSD has a linear time dependence

$$MSD = 2Dtd \tag{2.3}$$

in the 2D case $d = 2$, since it denotes the dimension of the system and D is the diffusion coefficient. Therefore, the diffusion coefficient is calculated from the slope of the MSD. The diffusivity appears also in the probability distribution function of particles with Brownian motion

$$\rho(r,t) = \frac{\rho_0}{\sqrt{4\pi Dt}}\, e^{-\frac{r^2}{4Dt}} \tag{2.4}$$

where $\rho(r,t)$ indicates the density of diffusing particles. This Gaussian distribution becomes broader as D increases, which means that with higher diffusivity more particles can diffuse far away from the initial position. Due to its meaning, the diffusion coefficient serves as an indicator of the particles mobility. Evaluating the MSD doesn't only give a measure of the diffusivity, it is used to classify the dynamics of the system. Indeed, thermal effects lead to diffusion regimes and the time dependence of the MSD reveals the kind of motion, as visualized in Fig 2.1. Normal diffusion refers to the type of motion described by Brownian motion, so the MSD has linear time dependence. While in directed motion, particles are subject to an external force, which causes particles to move with a constant velocity and the MSD to be quadratic with respect to time. The other two regimes that can be distinguished with the MSD plot are the anomalous subdiffusion and the confined motion. In the former, particles move more slowly than in the normal diffusion case due to obstacles. Whereas if the movement is limited to a finite space, the MSD reaches a plateau over time, and the motion is identified to be confined.

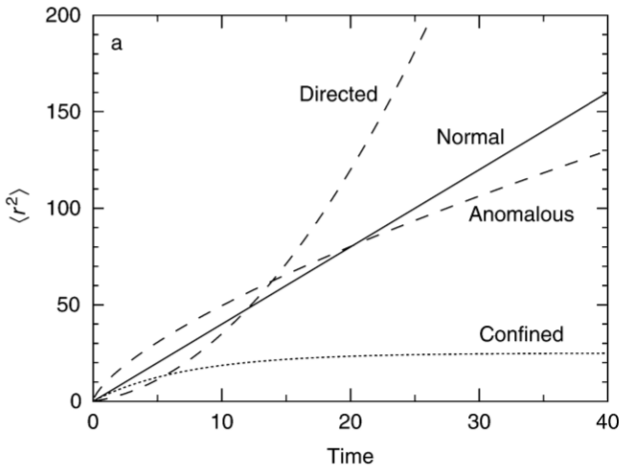

Figure 2.1: Mean Square displacement as a function of time for normal diffusion, anomalous subdiffusion, directed motion, and confined motion [16].

To analyze the particle trajectories, we have used a MATLAB class, the MSDanalyzer [17], that computes automatically the MSD and the D from the tracks. In each track are stored the positions in time of skyrmions, and the MSDanalyzer also allows plotting the tracks, as visualized in Fig 2.2. The stochastic nature of skyrmion motion is clear, and to better understand it, the MSD is extracted for each track.

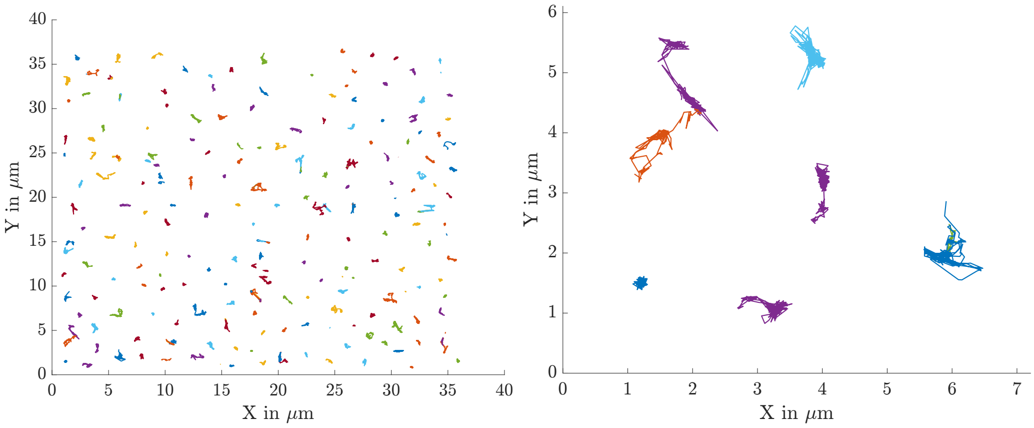

Figure 2.2: Plot of the skyrmions tracks in a $40 \times 40\,\mu m^2$ irradiated square, extracted using the MSDanalyzer [17]. On the right there is a zoom on the tracks, as to appreciate the random nature of the skyrmion motion and the uniqueness of each skyrmion's displacement. Indeed, one skyrmion is moving less than the others.

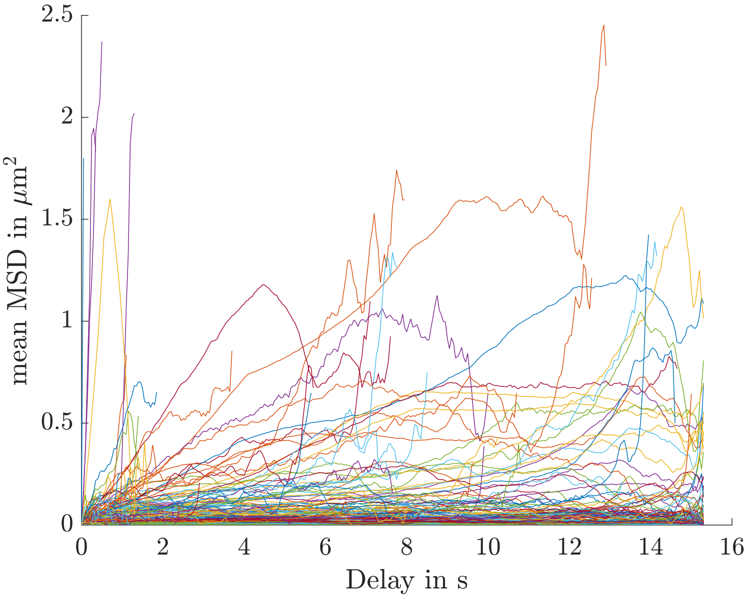

Figure 2.3: Plot of the time averaged MSD for each skyrmion trajectory in the irradiated square of Fig 2.2.

The heterogeneity of skyrmions movements is visible in Fig 2.3, some tracks are shorter in time but with large displacement, while others that are lasting longer have very little displacement. Extracting the average of the MSD curves, as in Fig 2.4, means describing the motion of the ensemble, and the resulting behavior comes from the dominant trait of the whole. In the following sections, the reasons for the effects of irradiation are concluded on the mean of the MSD curves.

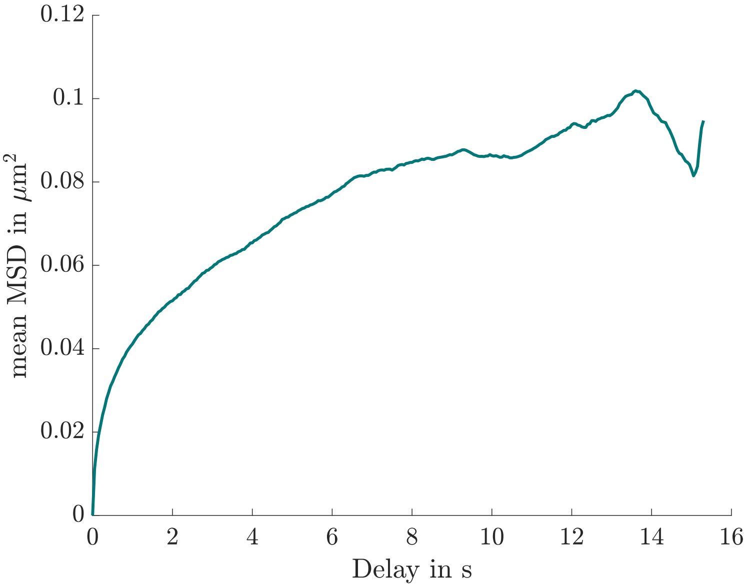

Figure 2.4: Plot of the ensemble average of the MSD of Fig 2.3.

2.3 Recording skyrmion motion

A high temporal resolution camera integrated with a wide-field magneto optical Kerr microscope WMOKE has been used to capture skyrmion motion. The PCOcam software records the movie, which is a sequence of images with a pixel size $51.2 \times 51.2\,nm^2$, determined by the 50x objective lens of the WMOKE. We have tuned the camera exposure time. It is the time of light exposure for the camera's sensor when capturing an image. If it is short, the light may be insufficient to capture the contrast of the image. Whereas, if the exposure time is longer the contrast is improved, as it appears in Fig 2.5.

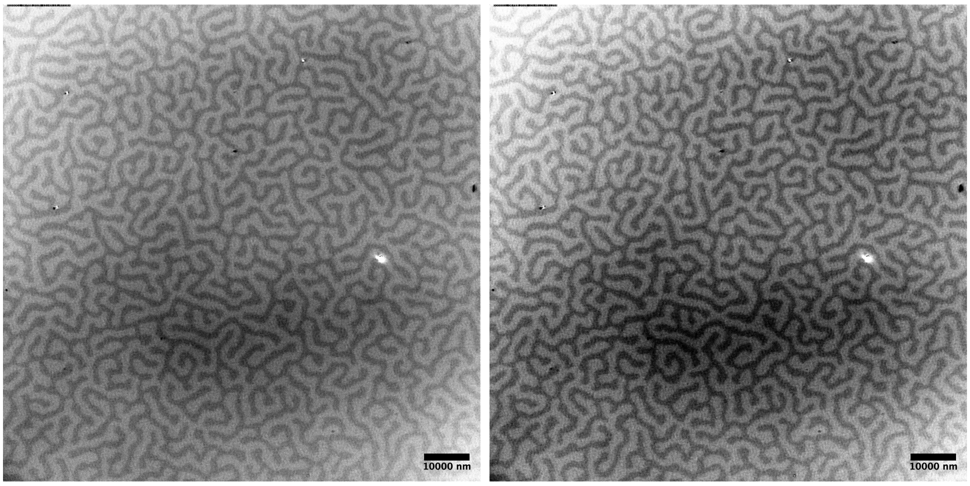

Figure 2.5: The frame on the left is of a movie recorded with an exposure time of $100\,ms$, while on the right an exposure time of $200\,ms$ is used.

Contrast enhancement comes at the cost of losing time resolution, since with long exposure time the details of the motion could be missed between frames. For the sake of the dynamics accuracy, a short time exposure of $50\,ms$ is chosen, and the movies are recorded for 15 seconds, which corresponds to 300 frames. Due to the low contrast, the movies have been processed using Fiji, an image processing package distributed by ImageJ [18]. The first amelioration consists in subtracting an image of the saturated magnetic structure to the images in the video. Hence, better contrast and the cancellation of defects on the thin film are achieved. This is fundamental because the tracker could mistake the defects for skyrmions. Then a band pass filter is applied, which removes high spatial frequencies (blurring the image) and low spatial frequencies (similar to subtracting a blurred image).

2.4 Tracking with TrackMate

Manipulating the image quality is important because the tracking tool provided by Fiji, TrackMate [19], has to identify a skyrmion in one frame and link it to skyrmions in the preceding and successive frames. Therefore, the skyrmions features should be as pronounced as possible, in order to avoid false linking between frames.

The tracking scheme is divided in two separated steps: detection and particle-linking. The detection algorithm that is best suited for Gaussian-like particles such as skyrmions, is the DoG (Difference of Gaussian) detector. It works by applying two Gaussian filters with different standard deviations to the image and then subtracting the results. In this way it returns smooth images with sharp local maxima at skyrmion locations.

Whereas the chosen particle-linking algorithm is the Linear Assignment Problem (LAP). The reason behind this choice is the possibility of tuning gap closing events that the LAP offers. A skyrmion can disappear for one or more frames and with this feature the tracker manages to reconnect reappearing spots. To exclude physically unreal connections, we must introduce limits that exclude every skyrmion to link to every other skyrmion or track segment. These cutoffs are based on the distance that a skyrmion can cover and are set to values coherent to the observed motion. The tunable parameters for this algorithm are three.

- The **frame to frame linking distance** is the maximum distance that an object can cover between two consecutive frames. Its value has to be carefully chosen because if it is either too short or too long, one obtains fake tracks.
- The **gap closing distance** defines the spatial range for detections across multiple frames as to allow the tracker to close the gap between them.
- The **maximal frame interval** accounts for the duration of disappearance events. It sets the maximum number of frames to use for bridging two skyrmions.

2.4.1 Tuning TrackMate parameters

The DoG has estimated that in our magnetic thin film the skyrmion diameter is circa $1200\,nm$. Observing the skyrmion motion, their average displacement between two frames is circa equal to their diameter. To decide which value to use for the gap closing distance, movies of skyrmions with different ion doses are recorded, processed with TrackMate and then the tracks with different gap closing distance are extracted. The idea is to get the diffusivity of skyrmions tracks that use different gap closing distances, compare them and verify which parameter gives results closer to the observed motion.

Increasing the gap closing distance, skyrmions with higher diffusivity are less often lost in the tracking, thus we expect higher diffusivity for high gap closing distances.

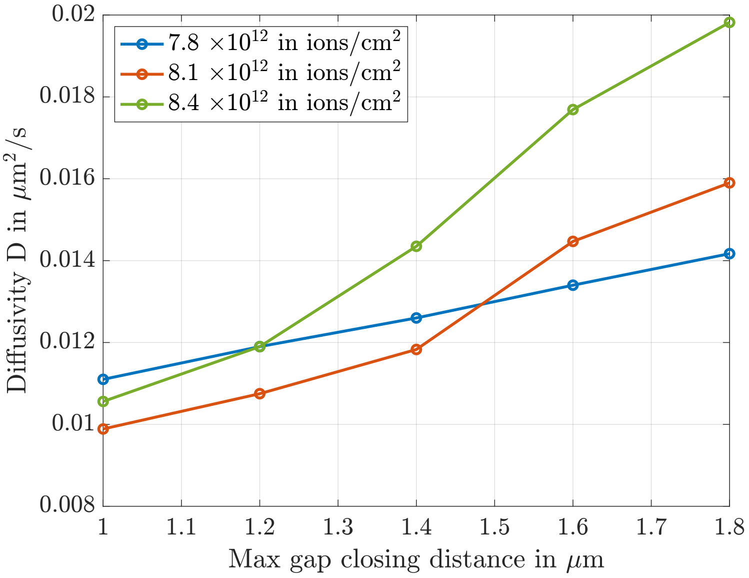

Figure 2.6: Comparison of diffusion coefficients for different gap closing distances at different ion doses.

From Fig 2.6, it is clear that for gap closing distances lower than 1600 nm skyrmions at higher ion doses result a lower diffusivity. This is not what we expected, since we have observed that for higher ion doses, skyrmions exhibit greater mobility. Hence, we assumed that with short gap closing distances, the tracker can not properly follow the faster moving skyrmions. When increasing the gap closing distance beyond 1600 nm, a more precise tracking is evident and the diffusivity values follow the trends observed by inspection. Gap closing distances higher than 1800 nm were considered as well; but inspecting the tracks we found false connections between tracks belonging to different skyrmions.

On the other hand, the choice of the particle linking distance was made evaluating the variation in the measurements with a ±20% change of the frame to frame linking distance. The result is that the diffusivity changes less than 4%. This is a reasonable variation because it is in the same order of magnitude as the change of diffusivity belonging to skyrmions of different ion doses. Because of this, we employed a linking distance equal to the estimated skyrmion diameter.

Moreover the skyrmion density in the irradiated square depends on the used ion dose. For low ion doses there are few skyrmions, sometimes also mixed with domains, while at high ion doses the skyrmion density increases a lot. When the density of objects to be connected is high, the number of potential assignments increases as well, making it more difficult for the tracker to not create false linking. According to [20], the tracker performs best for the lowest-density simulation and the efficiency decreases with higher densities. They have checked the goodness of the LAP algorithm concerning the density of particles with five simulations of increasing particle density. By looking at the percentage of true and false particle linking in Fig 2.7, even though the fifth simulation (highest particle density) has circa 40% of particles with nearest neighbors closer than twice their average displacement, only 10% of the links are false. The percentage of wrong gap closing events is higher, but still acceptable. This proves the power of the tracking approach and that we can trust the skyrmion trajectories for both low and high ion doses (low and high skyrmion densities) conditions.

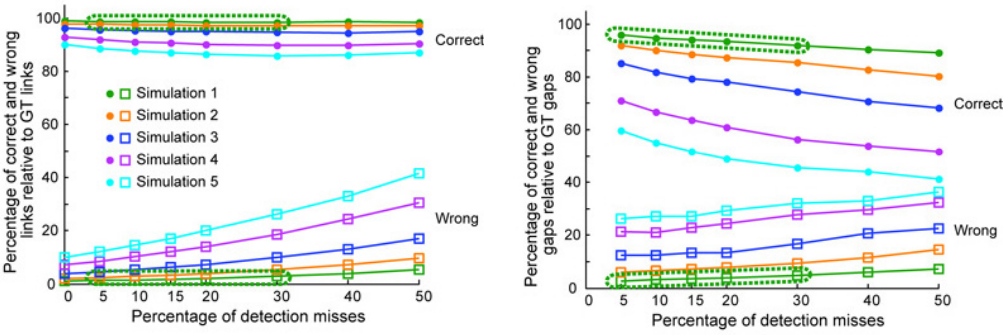

Figure 2.7: Five simulations of increasing particle density have been used to validate the tracking algorithm. On the left, there is the percentage of true and false positives in particle linking, and on the right in gap closing [20].

2.5 Skyrmion motion type analysis

The investigated skyrmion motion was observed in the $W_{(3)}/CoFeB_{(1)}/MgO_{(1)}/Ta_{(3)}$ stack, where $80 \times 80\,\mu m^2$ squares were irradiated with varying ion doses and beam currents. We focused our analysis on the squares patterned with a 7.7 pA ion beam current, and recorded skyrmion motion in five squares with ion doses ranging from 7.8×10^{12} ions/cm^2 to 9×10^{12} ions/cm^2.

2.5.1 Evaluation of the MSD

First, we investigated the behavior of skyrmions at the same ion dose with different magnetic fields. The range of magnetic field is not the same for all the ion fluences, since for higher doses skyrmions are more stable against higher magnetic fields, while at lower doses they annihilate with lower magnetic fields.

As it shows in Fig 2.8a with an external field of 0.5 mT, the mean MSD evolution in time has a linear development, and it is similar to the case of normal diffusion shown in Fig 2.1. Whereas, at 0.6 mT, the MSD profile suggests that skyrmions move in a confined way. Confined diffusion behaves as normal diffusion at short times but at long times the MSD approaches a plateau. Indeed, with the microscope, we observed that skyrmions' motion is restricted to a certain region. What stands out in Figs 2.8b–2.8d is the same trend described above but occurring more pronounced at higher fields as the higher ion doses allows. Thus, skyrmions motion passes from freely diffusive to confined when the external magnetic field is increased for different ion doses. Our interpretation is that at high fields more diffusive skyrmions annihilate, while the pinned skyrmions at pinning centers dominate the system dynamics. In addition to the field effect, we must consider also that higher ion doses return a more diffusive behavior, which will be discussed in more detail in section 2.5.2. This higher diffusivity might stem from a reduction of pinning, so to understand this trend, we must delve more into the nature of pinning centers and the behavior of skyrmions in their presence.

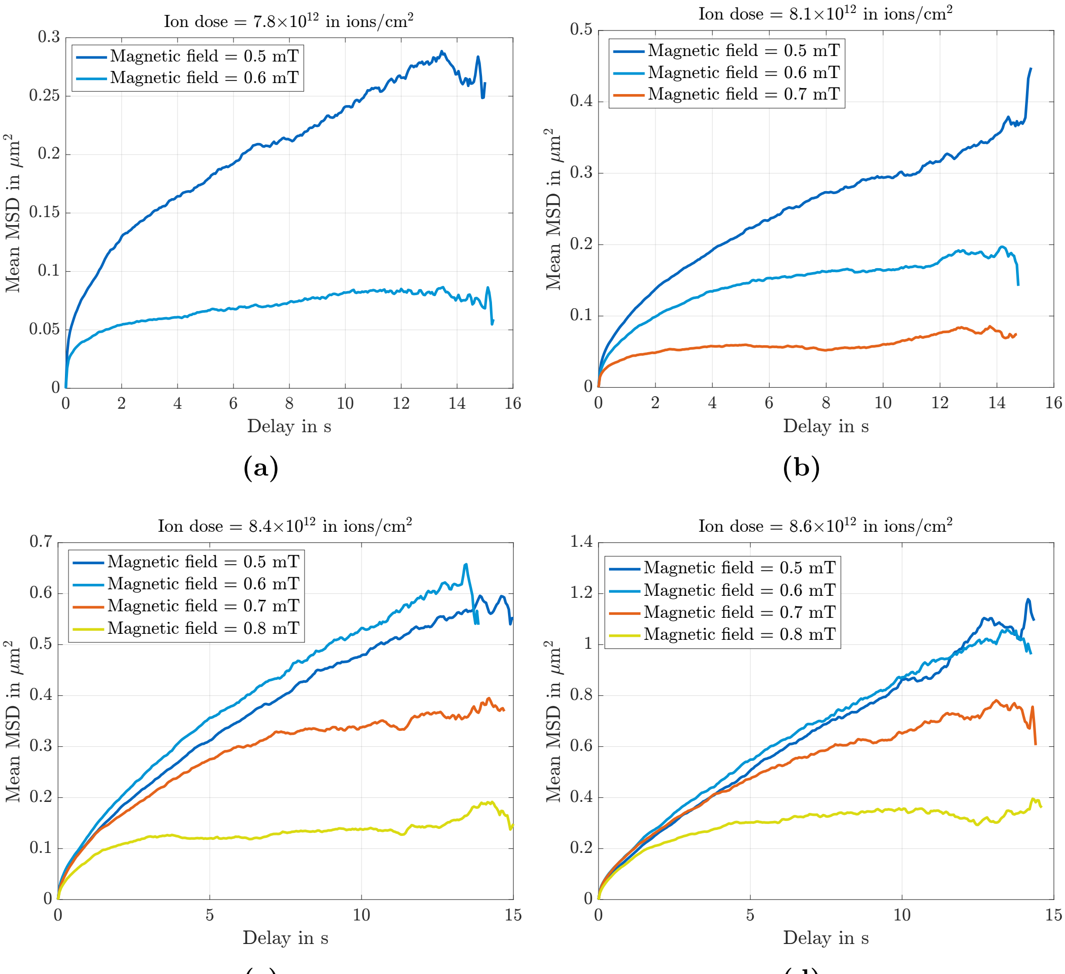

(a) **(b)**

(c) **(d)**

Figure 2.8: MSD curves for different magnetic fields and at the following ion doses: a) $7.8 \times 10^{12}\,\text{ions/cm}^2$, b) $8.1 \times 10^{12}\,\text{ions/cm}^2$, c) $8.4 \times 10^{12}\,\text{ions/cm}^2$, and d) $8.6 \times 10^{12}\,\text{ions/cm}^2$. For each ion dose skyrmions' motion is analyzed for the magnetic fields at which they appear, and for lower magnetic fields a more diffusive behavior (corresponding to linear MSD(t)) is consistently retrieved changing the ion dose.

2.5.2 Skyrmion pinning

Pinning is a trapping force that strongly reduces the skyrmions mobility and forces skyrmions into energy minimizing regions, the pinning sites. This inhomogeneous energy landscape of skyrmions happens when different interactions on similar energy scale appear [21].

It is produced by variations in anisotropy, exchange interaction or DMI, missing spins, atomic impurities or surface adatoms that make the crystalline structure disordered. Defects can be either attractive or repulsive for the skyrmion [22]. The pinning interaction strength also depends on the difference in size between the skyrmion

and the defect, if the defect radius is larger than the one of the skyrmion, the dwell time of the skyrmion at the defect is increased. In the presence of pinning sites, the motion is a hopping diffusion, since the skyrmion moves between pinning sites.
Ga+ irradiation is a powerful tool to tune the strength of pinning sites. Indeed, in a magnetic stack like the one under study, a plausible cause for the presence of pinning centers is the formation of atomic steps. Those originate at the W/CoFeB interface during the deposition process.
Thanks to ion irradiation, atomic steps are partially substituted by intermixing of atomic species [23]. The interface disorder doesn't disappear, but after irradiation it is lowered, producing a reduction of pinning effects at higher ion doses.

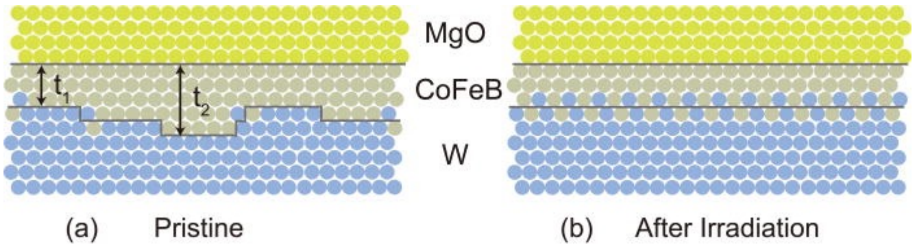

Figure 2.9: Schematic of the interface structure in (a) pristine and (b) irradiated W/CoFeB/MgO films [23].

By plotting together the MSD curves ofof skyrmions in a film treated with different ion doses at the same magnetic field, a transition from confined to free diffusion for higher doses occurs (as in Fig 2.10a). The MSD is more linear, proving that skyrmions can move with Brownian motion once the ion dose is high enough to contrast pinning effects. In Figs 2.10b–2.10c skyrmions at high doses keep showing more diffusive behaviors, and it also clear the increase of magnetic field at which skyrmions annihilate. Especially for 0.8 mT (Fig 2.10d), only in three of the five probed squares skyrmions are present and their motion is confined since only pinned skyrmions are left.

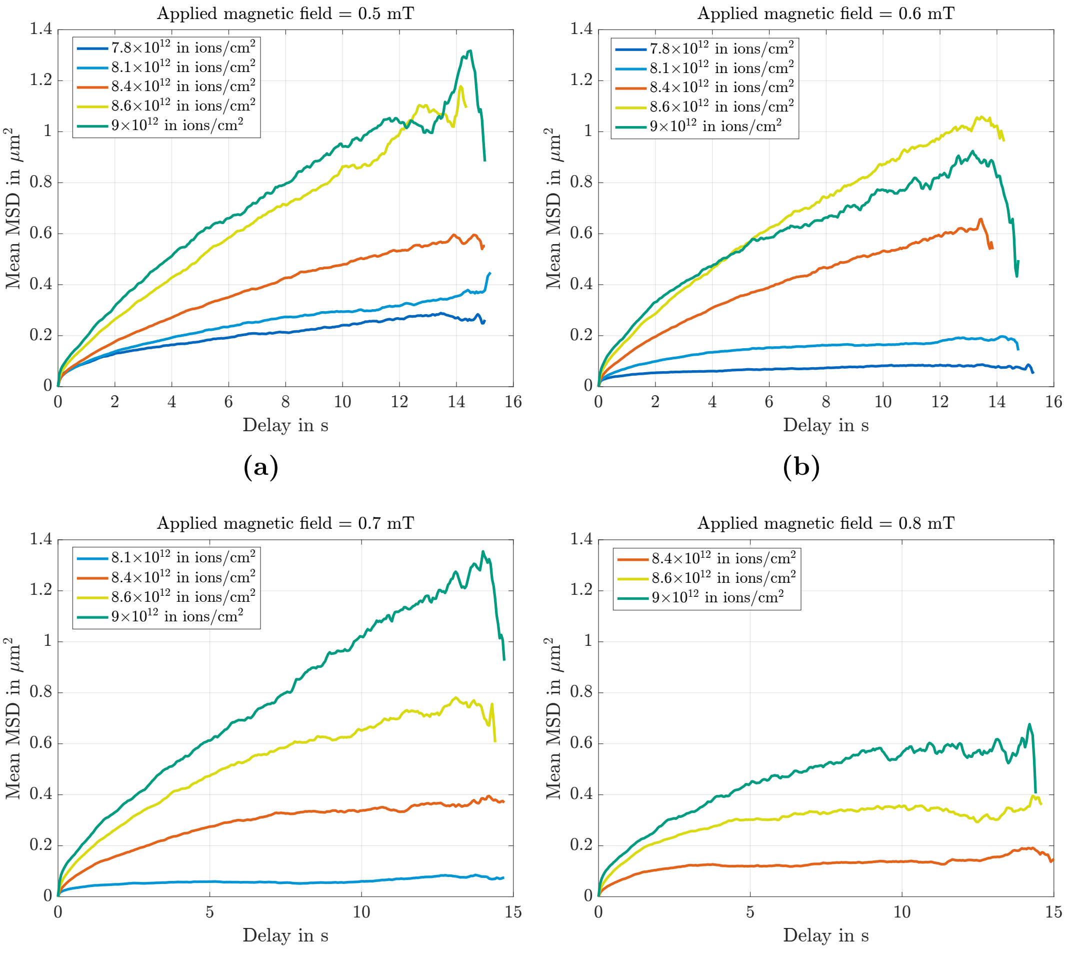

(a) **(b)**

(c) **(d)**

Figure 2.10: MSD curves at different ion doses for fixed magnetic fields. a) By looking only at the effect of changing the ion doses and keeping the same magnetic field (0.5 mT), it is clear that at higher ion doses skyrmions are freely diffusing and at lower ion doses their motion is restricted. The same trend is retrieved in b) at 0.6 mT and c) at 0.7 mT. Whereas in d) for 0.8 mT skyrmions' motion is confined for all the analyzed ion doses, since at this magnetic field only pinned skyrmions are left.

The comparison between the shapes of the tracks in Fig 2.11 and in Fig 2.12, which are respectively at 7.8×10^{12} ions/cm^2 and 9×10^{12} ions/cm^2, serves as another indication of the diffusion enhancements obtained with more ion irradiation. Indeed, when the highest ion dose is used (Fig 2.12), skyrmion tracks are overlapping because while diffusing, skyrmions cover longer displacements and explore the space previously occupied by just one skyrmion. Meanwhile, at lower ion dose in Fig 2.11, the tracks of skyrmions are well separated, suggesting that they diffuse in a smaller area and most of them are pinned, since skyrmions remain fixed at the pinning center.

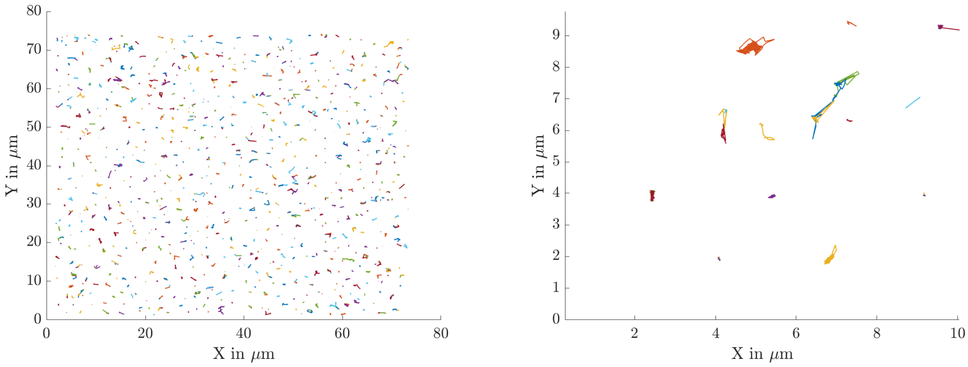

Figure 2.11: Plot of the skyrmions tracks in a $80 \times 80\,\mu m^2$ square irradiated with 7.8×10^{12} ions/cm^2 and at 0.6 mT. On the right there is a zoom on the tracks, which allows to see that skyrmions are diffusing with small displacements.

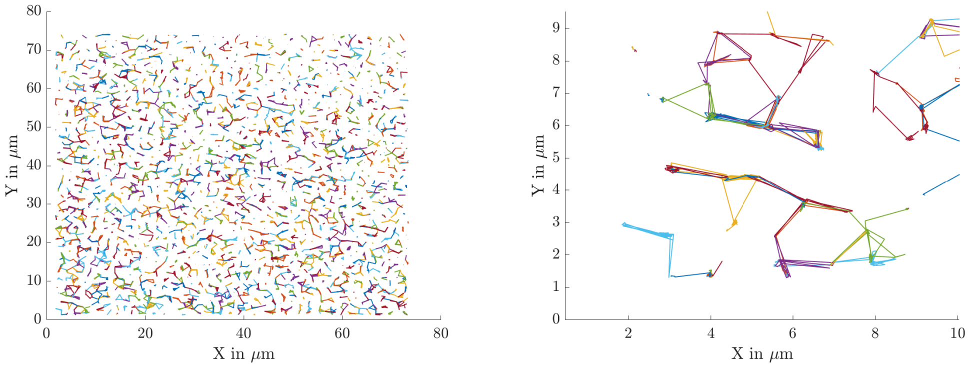

Figure 2.12: Plot of the skyrmions tracks in a $80 \times 80\,\mu m^2$ square irradiated with 9×10^{12} ions/cm^2, and at 0.6 mT. On the right there is a zoom on the tracks, which is included to visualize the greater displacement of skyrmions when those are in a state irradiated with higher ion dose.

2.5.3 Odd diffusion

Another aspect to consider is the increase of skyrmion density related to higher ion doses [10]. In these conditions, the space available for skyrmion motion is reduced and more skyrmion-skyrmion interactions are expected to limit the skyrmion movement. Therefore the enhancement of free diffusion for high ion doses is counter-intuitive with respect to the increase of skyrmion density. Not only pinning reduction is responsible for this unexpected trend, indeed another probable explanation is a dynamic effect, known as odd diffusion. When odd-diffusive particles collide, rather than hinder their motion, they move around each other. It is called "mutual rolling effect". Thus the increase in diffusion for higher density systems suggests that the mutual rolling effect counteracts the slowing down due to many-body interactions. This kind of motion is studied by [24] in systems with broken time-reversal, and might also apply to systems that are hosting skyrmions.

2.5.4 Motion type analysis through log-log fitting

The MSD curve for confined motion is situated below its tangent, which represents the curve in case of free diffusion. Therefore, if the MSD curve is modeled by a power law

$$MSD(t) = \Gamma\, t^{\alpha} \tag{2.5}$$

we could extract the exponent α and differentiate the motion by its value: with pure diffusion $\alpha = 1$ as it is clear from the MSD linear time dependence in Fig 2.1, while for confined motion $\alpha < 1$. The MSDanalyzer tool offers a log-log fitting to determine α: the power law can be turned in a linear law through a linear fit of $log(MSD)$ with respect to $log(t)$

$$log(MSD) = \alpha\, log(t) + log(\Gamma). \tag{2.6}$$

Before fitting, the tracks are filtered, because some of them are too short and to obtain a good enough fit, we use only tracks with more than eight points.
This analysis was conducted only for the skyrmions that showed confined motion from the MSD plots, as an additional proof. For each of these measurements, the mean α and the standard deviation are calculated, and then the distribution of the α values is plotted as in Fig 2.13. Since $\alpha < 1$, the motion of skyrmions in a film treated with 7.8×10^{12} ions/cm^2 at 0.6 mT is indeed confined.

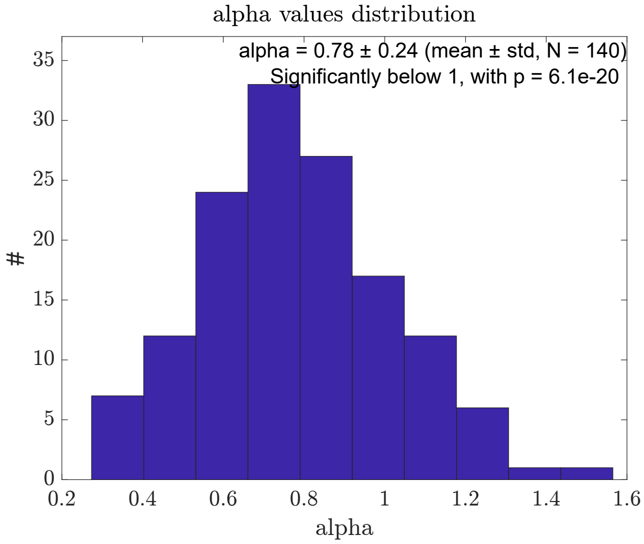

Figure 2.13: Alpha values distribution for skyrmions moving in an irradiated square at $7.8 \times 10^{12}\, ions/cm^2$ and 0.6 mT. The extracted mean alpha value and its standard deviation are: 0.78 ± 0.24.

Having identified two other cases of confined motion from the shape of the MSD(t), for those, the motion type analysis has been conducted through log-log fitting. The results are presented in the Table 2.1, and in both cases $\alpha < 1$, confirming the results of the previous evaluation.

Magnetic field in mT	mean(α) ± std(α)
0.6	0.78 ± 0.29
0.7	0.83 ± 0.30

Table 2.1: Table of the α values for skyrmions moving in an irradiated square with $8.1 \times 10^{12}\, ions/cm^2$ at 0.6 mT and 0.7 mT, which are showing confined motion.

2.6 Calculation of the diffusion coefficient

Before proceeding with the discussion about the diffusivity values, it is crucial to reflect on the method used for estimating the diffusion coefficient. Indeed, the latter is obtained fitting the MSD curve, which is not a trivial object since it is an ensemble average of time averaged curves. In the time average for each delay τ, the square displacement is averaged over all the time combinations that give that delay. For short delays there are more points to average than for longer delays, and this is even more accentuated for our tracks that are short. Taking as example the tracks of skyrmions in an irradiated state and producing the histograms of Fig 2.14, it is clear that most of the tracks start from the first frame but are not as long as the whole sampling time. Indeed for this case under analysis, there are 2018 tracks and 745 of them are just 0.5 seconds long.

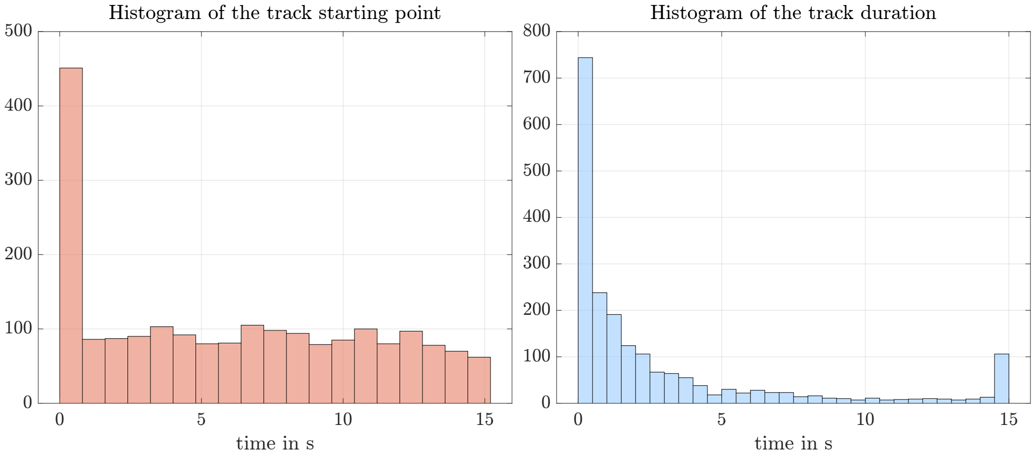

Figure 2.14: Histograms showing how many tracks start from the first frame and how long the tracks are. These tracks belong to skyrmions in films irradiated with $8.4 \times 10^{12}\, ions/cm^2$ at 0.8 mT.

Consequently, the MSD can't be trusted for long delays and the recommended strategy to extract correct data is to fit only the first 25% of the MSD curve [25]. Another indication that the behavior for long delays is inaccurate can be found in Fig 2.10, for any applied field the MSD curves at long delays have ripples that deviate from the trend at lower delays.

As suggested in the MSDanalyzer [17], when dealing with confined motion the fitting of the MSD curve should be even more restricted. For this reason, when we identify from the MSD plot that skyrmions are moving with confined motion, the diffusivity is evaluated using only the first 15% of the curve, which corresponds to the linear part of the curve.

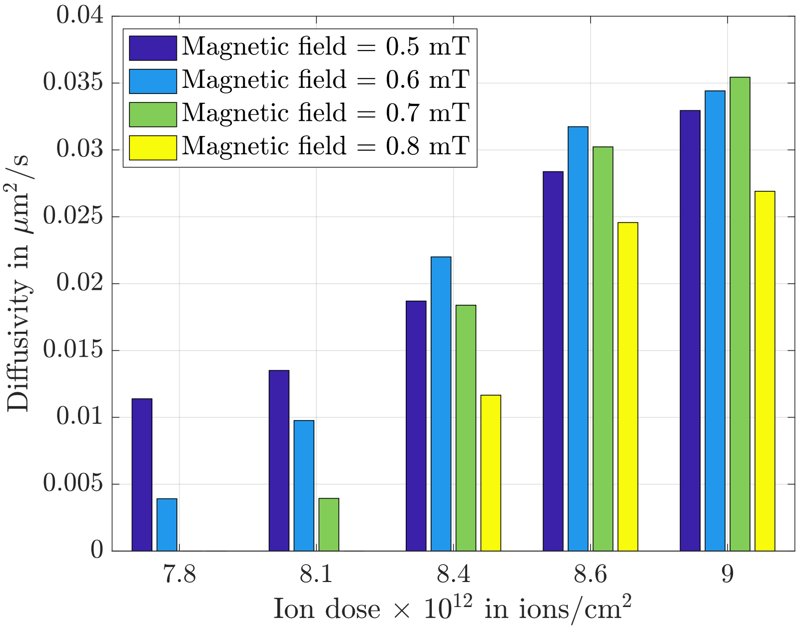

Figure 2.15: Bar plot of the calculated diffusivities at different ion doses and different magnetic fields.

In Fig 2.15 it is visible that for each magnetic field the diffusivity increases for higher ion doses. Also the transition from free diffusion behavior to confined motion that happens at higher magnetic fields is reflected on lower values of diffusivity.
The changes of the diffusion constant indicate the effects of ion irradiation on skyrmions, indeed at higher ion doses pinning centers are reduced, thus skyrmions are more free to diffuse, and their diffusivity increases. With respect to other studies on magnetic skyrmion diffusion, the same method has been used to retrieve the diffusivity but the conditions of the system are different.
In [13], they have carefully tuned the density of skyrmions as to avoid skyrmion-skyrmion interactions, and obtained $D = 0.27\,\mu m^2/s$. It is one order of magnitude higher than our best results, probably due to the possibility of tracking fewer skyrmions and not dealing with an ensemble. Another study [26], dedicated to the control of skyrmion bubbles diffusion through bias voltage, obtained $D = 0.11\,\mu m^2/s$. It follows that skyrmions in ion irradiated states with Brownian motion show less diffusivity with respect to the other studies, but in this case there is the advantage of tuning the diffusion with the amount of implanted ions, which is yet not explored in research.

2.7 Current driven skyrmion motion

After the characterization of Brownian motion, we proceeded to analyze the directed motion of skyrmions, passing a current through the sample.
Clamping the sample with metal contacts, a DC current is applied. The goal is to observe the transition from diffusive motion to a transported one and to distinguish this kind of movement employing the MSD curve. The Fig 2.1 shows that for directed motion the MSD must have a clear positive curvature. Comparing the shape of the tracks when a current is applied (Fig 2.16) and without current (Fig 2.2), it is apparent that the tracks are longer, indicating that skyrmions motion is no more just random; there is directionality.

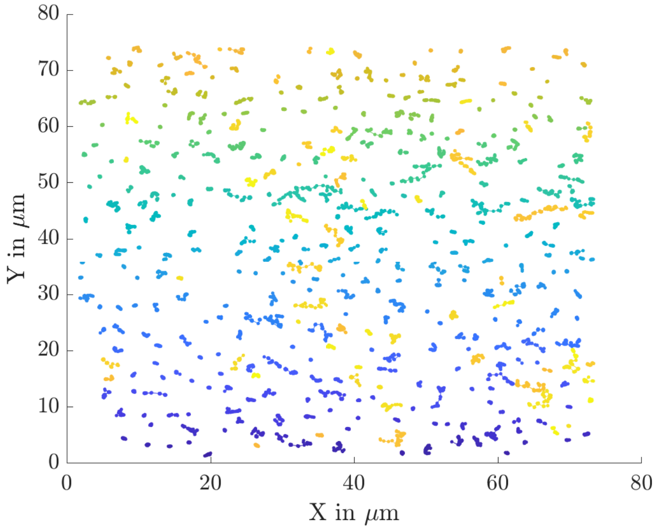

Figure 2.16: Plot of the skyrmion tracks in a $80 \times 80\,\mu m^2$ square irradiated with $7.2 \times 10^{12}\,ions/cm^2$ when a DC current of 8 mA is applied.

The motion was recorded applying both 8 mA and 10 mA for 15 seconds; with 8 mA skyrmions acquire more speed and transported motion is replacing the erratic Brownian motion, while directionality is fully achieved with 10 mA. Indeed, the typical parabolic behavior of transported motion is evident in the MSD plot for 10 mA in Fig 2.17, while for 8 mA the MSD curve is slightly different than the diffusion case, especially because here the behavior is consistent also for long delays. We have not analyzed higher currents because then skyrmions were very fast and both the optical resolution of the system and the time resolution of the camera were not enough to follow the skyrmion trajectories. For the same reason, the investigation was restricted to skyrmions in squares with lower ion doses, in which the skyrmion density is reduced and tracking skyrmions is achieved with more accuracy.

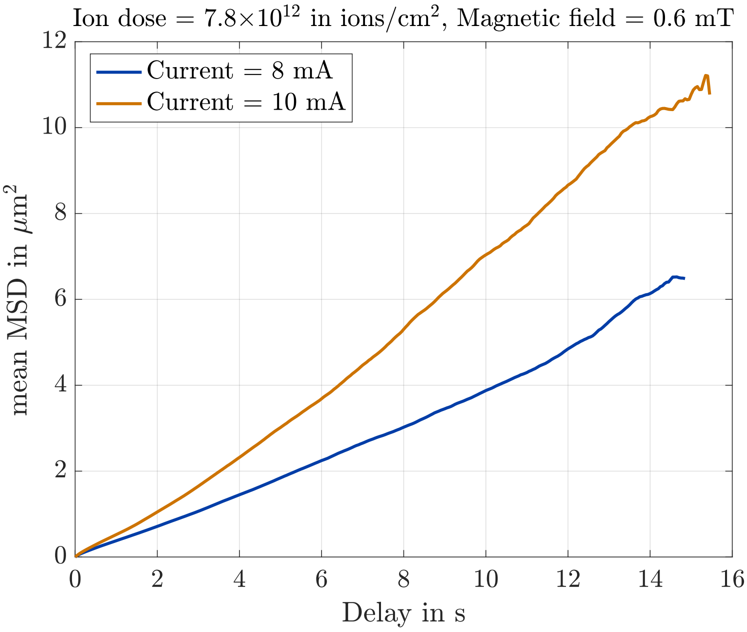

Figure 2.17: MSD curves when DC currents of 8 mA and 10 mA are applied.

Using a DC current of 10 mA is enough to achieve directionality, thus to study the relation between ion doses, applied magnetic fields and current we stick to this value. As prior to current application, for higher ion doses the motion is less constrained by pinning. In Fig 2.18d even though the ion dose is higher, the MSD curve shows a lower slope than the one of skyrmions at the same field and lower ion dose (Fig 2.18c). This data tells us that skyrmions are moving less with an ion dose of 8.1×10^{12} ions/cm^2 and it is not coherent with what we observed at the microscope, because we clearly perceived that the current transports skyrmions. The reason behind this result is that at 10 mA skyrmions acquire more velocity and at 8.1×10^{12} ions/cm^2 the density of skyrmions increases to a point that tracking is unreliable even with the best time resolution achievable in the setup.

All in all, the data that we have collected is enough to state that employing a current, on top of the fluctuation typical of Brownian motion, in ion irradiated states skyrmions can be moved and that transported motion is controllable by ion dose.

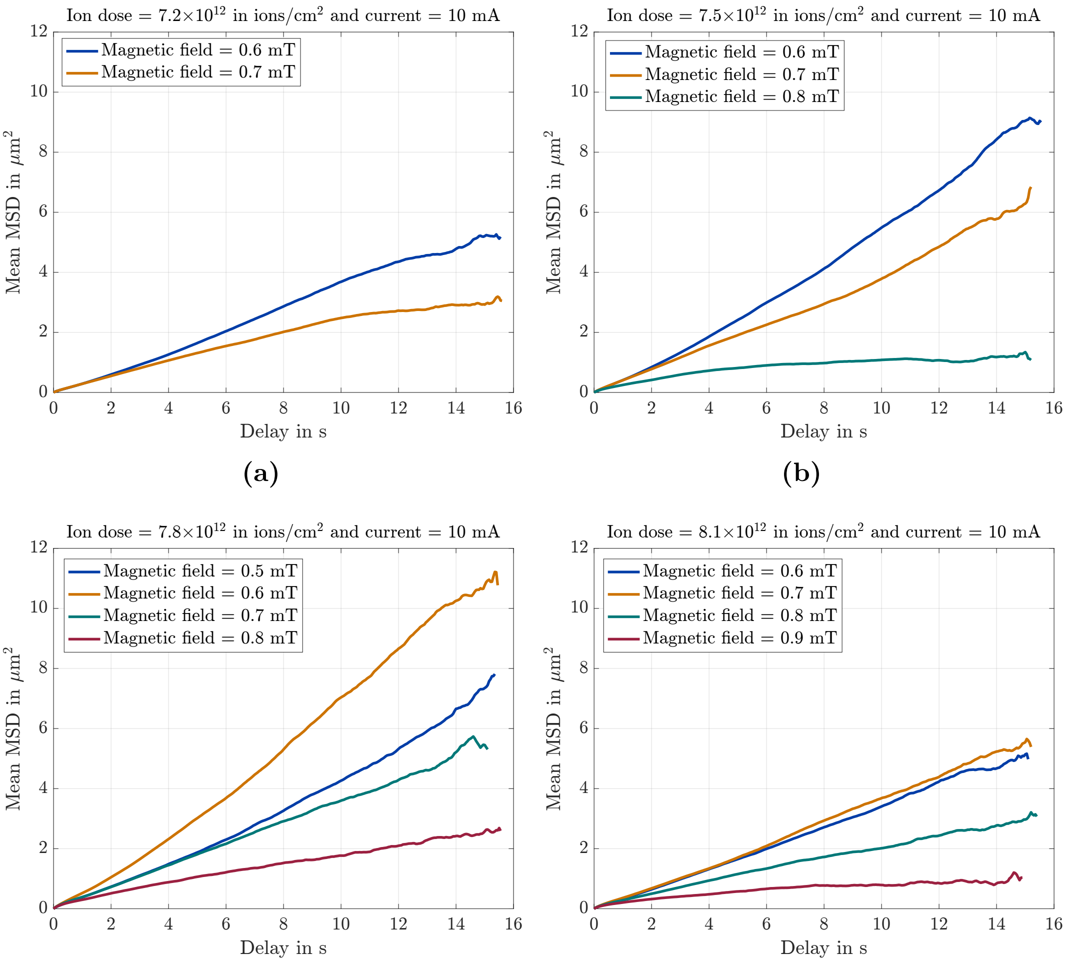

(a) **(b)**

(c) **(d)**

Figure 2.18: MSD curves at different magnetic fields for fixed ion doses when a direct current (DC) of 10 mA is applied. a) 7.2×10^{12} ions/cm^2, b) 7.5×10^{12} ions/cm^2, c) 7.8×10^{12} ions/cm^2 and d) 8.1×10^{12} ions/cm^2. For all ion doses the MSD slope reduces with increasing fields. While for increasing ion doses the MSD slope is higher, however this is not seen for d) because the tracker is no longer able to follow the skyrmion motion.

It is interesting to inspect the change in diffusivity when skyrmions are driven by a current. In this case, given the change to a parabolic shape of the MSD

$$MSD(t) = 2dDt + v^2t^2 \tag{2.7}$$

the average MSD curve is fitted with a polynomial.

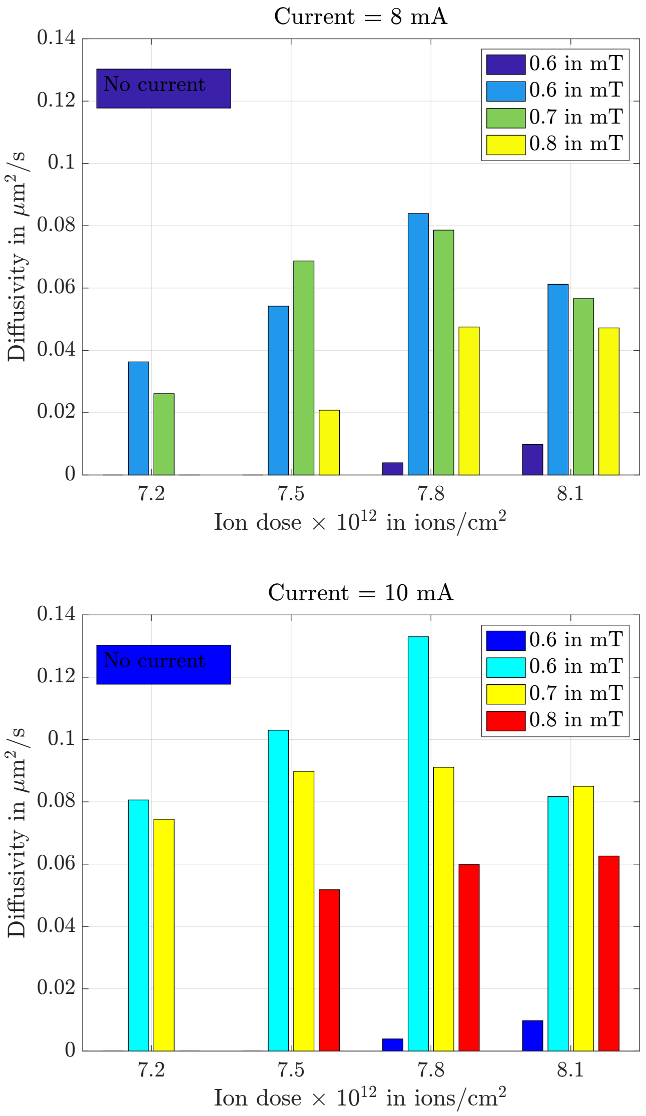

Figure 2.19: Bar plots of the calculated diffusivities at different ion doses and different magnetic fields, when a DC current of 10 mA is applied. The diffusion coefficient without current is taken for 0.6 mT, which represents the highest diffusivity for these ion doses and it is shown in this bar plot with the intent of highlighting the improvement in diffusivity with the current applied.

The high diffusivity values reflect the larger spatial extent of skyrmions displacement. What is striking in Fig 2.19 is the dominance of skyrmions with higher mobilities at lower magnetic fields, which are the same showing more directionality with applied current in the MSD plots in Fig 2.18. Moreover, the high difference in diffusivity with respect to the case without current, highlights the advantages of tuning skyrmions mobility in several ways.

2.8 Conclusions

This chapter investigated the Brownian motion of skyrmions and its variation upon ion irradiation in $W_{(3)}$/$CoFeB_{(1)}$/$MgO_{(1)}$/$Ta_{(3)}$. We have shown that ion irradiation can be used to improve the diffusion of skyrmions thanks to the reduction of pinning, because FIB induces intermixing at the interfaces of the stack. Our view is that ion irradiation can be used to change the diffusion regime, indeed by tuning the amount of ions skyrmions motion shifts from confined to diffusive. However, we have not explored the possibility of enhancing the diffusion of magnetic skyrmions through defects, as it was simulated in [27]. It could be the starting point of another analysis, to generate with the FIB inhomogeneities in the magnetic materials that have strengths near the depinning threshold, and use the same specific conditions, in order to record skyrmion Brownian motion and prove that it could be enhanced by defects.

Another interesting aspect, considered in this analysis, has been the increase of skyrmion density upon irradiation. It appeared to us that the increase of the density could have a part in the increment of diffusion, and the data reflect this assumption. Anyway, the high skyrmion density of our system makes more difficult to compare the results to previous studies that have evaluated the diffusion of skyrmions [13, 26], since those record the track of fewer skyrmions. Consequently, we conclude that since we are considering an ensemble, the extracted figures of merit, like the MSD and the diffusivity, are describing the most prominent behavior of the system. In the same irradiated squares, pinned skyrmions and high mobile ones coexist; a higher ion dose increases the number of diffusive skyrmions while for low ion doses pinning dominates the forces acting on the ensemble. Thus, the possibility of tuning the Brownian motion with irradiation makes the future use of diffusion as the driving force in a skyrmion device very interesting, because it works at room temperature, and the used fabrication techniques make it compatible with existing CMOS technologies.

Our set-up could be easily changed to apply a DC current, and the implemented method to record and then analyze Brownian motion was also ready to measure how the motion changes with a current and if it is directed. The reason why we conducted this analysis is that one of the best qualities that makes skyrmions suitable for logic devices is the possibility to induce their motion with a current, and it is interesting to explore the effects of irradiation on skyrmion transport. The result showed that skyrmions did not stop the fluctuations while the current passes through the sample, and on top of fluctuating, skyrmions moved thanks to the current until annihilating at the irradiated square edges. High current density also means an increase in temperature due to the Joule effect. In this thesis, the latter effect is not inspected, but it would be fascinating, since Brownian motion is dependent on temperature as well, and it may be another way to tune skyrmion diffusion.

Chapter 3

Gradient engineering

3.1 Fluctuations as a computing mechanism

In the previous chapter, we pointed out that the Brownian motion of magnetic skyrmions can be tuned with ion irradiation. The next step is to make use of Brownian motion as a driving force to dynamically modulate and redistribute information to change state, in other words, to perform some computation.

Brownian motion is inherent in biological organisms and it offers a free search mechanism, essential to increase routes, improve information transfer, assist in response trigger, and ensure variability. Digging more into biological examples that harness fluctuations to achieve their functions offers an opportunity to find a way to exploit diffusion as a useful resource also in our magnetic framework.

Among the biological activities aided by thermal diffusion, there is muscle contraction [28]. Myosin is a protein structure in muscle cells that diffuses while searching for the next binding site. The directional movement of muscle myosin is achieved thanks to an energy potential created by the interaction between actin and myosin. These two reacting molecules are brought closer by diffusion, so the random motion aids the directionality of the reaction.

Another example is found in the study of genetic regulatory circuits, which highlights that the stochastic production of proteins is the reason why subpopulations express alternative phenotypes, even in genetically homogeneous populations in identical environments, as it is pointed out by [29]. These two examples show that in different biological functions, random fluctuations are essential to achieve a purpose, and in both cases, noise is harnessed when it is biased. So, the potential function of the system must be modulated by a driving mechanism [30].

This concept, proposed in [31], is exploited for a Brownian motor driven by temperature oscillations. The potential's cycling, which provides the energy input, allows the directed motion of particles when combined with structural asymmetry and diffusion, as shown in Fig 3.1.

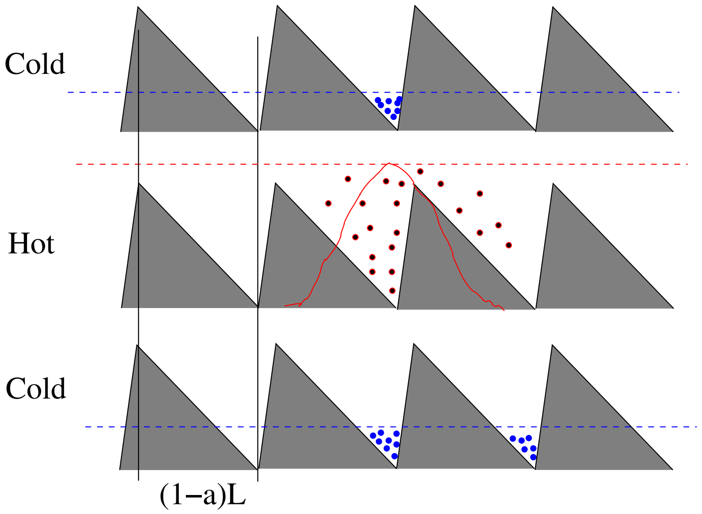

Figure 3.1: Working principle of a Brownian motor driven by temperature oscillations [31]. The asymmetry of the potential function allows the overall motion to be towards the right, because particles that diffuse towards the left should cover a larger distance, which is less likely to occur.

To sum up, the role of stochastic processes in biology is accomplished thanks to a bias that guides the randomness. On the account of this, to achieve an alternative driving mechanism based on the diffusion of magnetic skyrmions, our system must experience an asymmetry. Given the effects produced by different ion doses on the diffusion of skyrmions, we propose a gradient of ion doses to engineer the Brownian motion of skyrmions. Along the gradient, skyrmions should experience different conditions that lead to their net directed motion.

3.2 Tuning magnetic properties with Focused Ion Beam

To design the gradient, it is essential to understand which magnetic properties change upon ion irradiation, because their change influences skyrmions.

Gallium ions in Pt/Co/Pt samples show a reduction of crystalline anisotropy [32]. We assume that the same happens using our magnetic stack. The effect of irradiation on the interface DMI is studied with Helium ions irradiated on the Ta/CoFeB/MgO stack [33]. Enthalpy favors diffusion of Fe, Co, and B into Ta rather than MgO, making the Ta/CoFeB interface more exposed to intermixing. Therefore, the two interfaces have two different rates of intermixing, and this difference increases upon irradiation. The outcome is that DMI, which is an interface dependent phenomenon, increases with the ion dose. This result is considered valid also for irradiation with Gallium, paying attention that being heavier, Ga+ ions are stopped more efficiently and produce less damage to the underlying layers. Indeed, in our study of the magnetic phase for different ion doses (Fig 1.7), for higher doses there are more skyrmions, proving higher DMI and reduced anisotropy.

Both gradients with anisotropy and DMI have been simulated as the driving force for skyrmion motion [34]. The results of this study are of interest for this thesis because they show the skyrmions' behavior with respect to these changes and can help to predict how skyrmions diffuse in the gradient. The simulations show skyrmions moving in a straight line, similarly to Néel skyrmions driven by SOT, from regions of high anisotropy to regions with lower anisotropy. From this evidence, the gradient is designed to start with low ion doses (high anisotropy) and gradually change up to high ion doses (low anisotropy).

3.3 Ion doses maps

The sample where we conducted most of the irradiation with the gradients is slightly different than the one where we documented the Brownian motion of skyrmions. It has a different thickness of the Ta capping layer: $W_{(3)}/CoFeB_{(1)}/MgO_{(1)}/Ta_{(2)}$. This changes the ion dosages at which skyrmions appear and the range of magnetic fields that stabilize skyrmions. Since the gradients span over a range of ion doses, we irradiated ion dose maps to find this range where the effects of irradiation are suitable for the gradient. The input parameter that has to be inserted in the FIB and that allows tuning the amount of implanted ions is the dwell time. It represents the time that the ion beam remains in one spot. Moreover, we used the FIB with different combinations of ion beam currents and blur to control the dose and the homogeneity of irradiation. To finely inspect the ion doses, we employed the smallest ion beam currents of our instrument: 7.7 pA and 1.1 pA. Beam diameters of 7 nm and 5 nm (Fig 3.2) correspond to the selected currents.

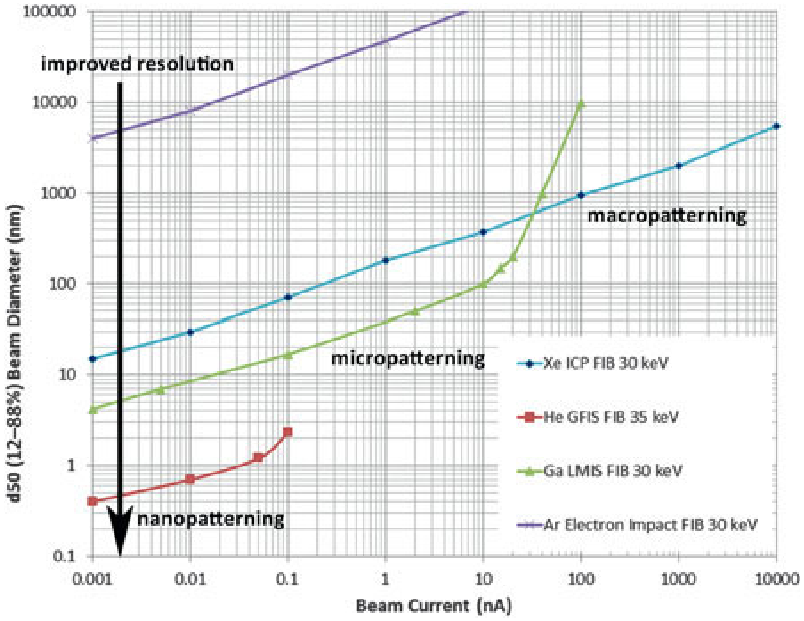

Figure 3.2: Beam size versus beam current graph of ions from different ion sources [35]. In the FIB we use a source of Gallium ions at 30 keV.

However, the diameter is also affected by the focus of the beam on the surface of the sample; to adjust the focus, the blur can be set. In the context of FIB, blur refers to the additional spreading of the ion beam spot beyond the ideal focused point. We chose to inspect the effects of 10 nm and 20 nm of blur.

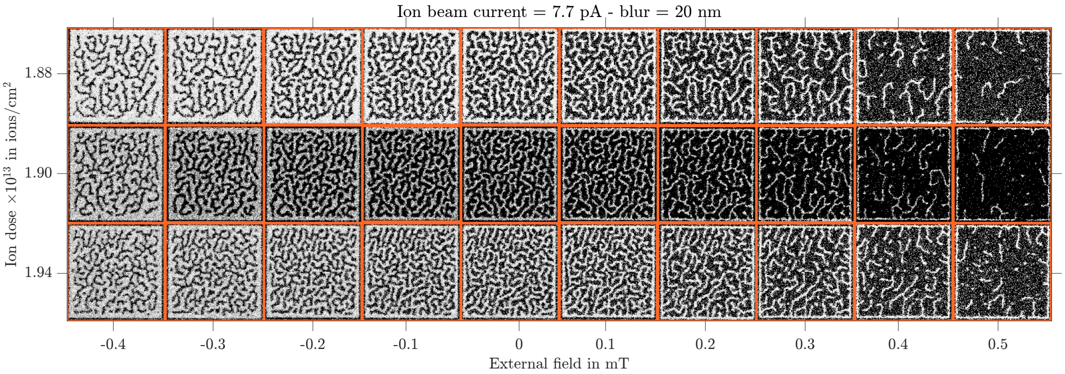

Figure 3.3: Magnetic phase diagram of domain structures in Ga-ion-irradiated $40 \times 40\,\mu m^2$ squares on $W_{(3)}$/$CoFeB_{(1)}$/$MgO_{(1)}$/$Ta_{(2)}$. The images of magnetic domain patterns are captured with a polar magneto-optical Kerr effect (MOKE) microscope.

Fig 3.3 depicts the evolution of magnetic domain patterns and skyrmions nucleation with different magnetic anisotropy given by different ion dosages. Through this evolution we checked the behavior upon irradiation and confirmed that at higher doses domains shrink and skyrmions are stabilized for higher magnetic fields.
To highlight the dependence of the ion dose on the current and dwell time, we report the analytic formula to calculate it

$$\text{Dose} = \frac{\text{Current} \times \text{Dwell time}}{\text{Area} \times \text{Elementary charge}}. \tag{3.1}$$

Then, we inspected the ion dose range obtainable with 7.7 pA and 20 nm of blur and that presents skyrmions.

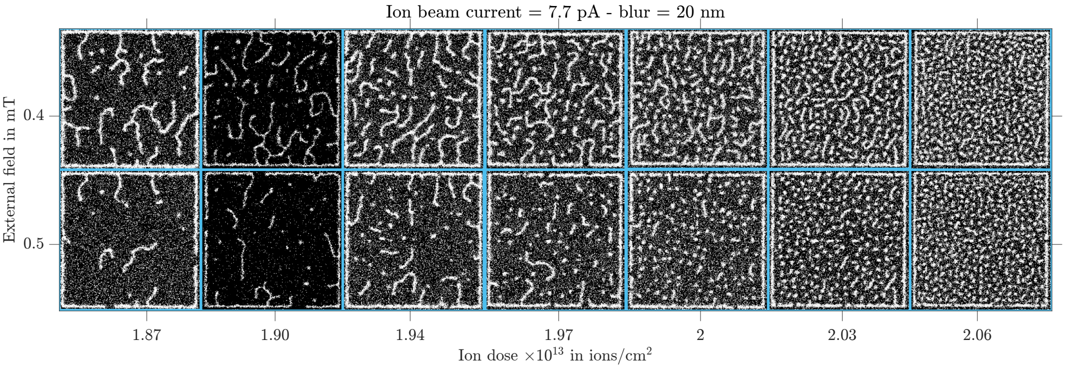

Figure 3.4: Evolution of skyrmion nucleation for different ion doses, using in the FIB settings 7.7 pA of ion beam current and 20 nm of blur.

As shown in Fig 3.4, for lower ion doses, skyrmions are mixed with domains and the density of skyrmions progressively grows with higher ion doses as well as the stability against external magnetic fields. We decided not to use ion doses higher

than $2.06 \times 10^{13}\, ions/cm^2$ because then the density of skyrmions is too high and their motion is dominated by skyrmion-skyrmion interactions.
As anticipated, we checked the effect of changing the ion beam current and the blur.

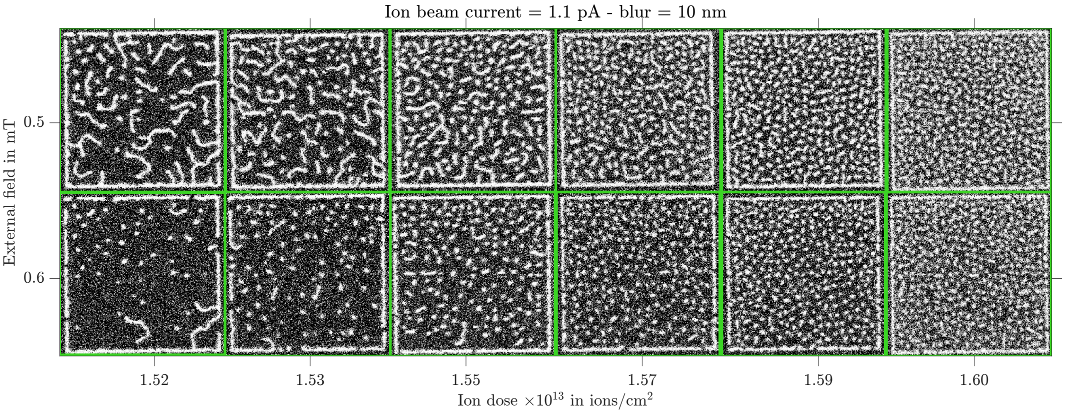

Figure 3.5: Evolution of skyrmion nucleation for different ion doses, using in the FIB settings 1.1 pA and 10 nm of blur.

With 1.1 pA, the range of ion doses has changed, our hypothesis is that a different way of implanting ions affects intermixing; thus the magnetic structure is stabilized by skyrmions with different amounts of ions. The different range of ion doses is visible in Fig 3.5. Moreover analyzing the case of 7.7 pA and 10 nm of blur, we noticed that for only three ion doses ($1.64 \times 10^{13}\, ions/cm^2$, $1.72 \times 10^{13}\, ions/cm^2$ and $1.80 \times 10^{13}\, ions/cm^2$) stable skyrmions are obtained.
Before moving on with the irradiation and analysis of gradients, we evaluated the Brownian motion for the skyrmions in these ion dose ranges. The motif of repeating this analysis is to have a direct comparison between skyrmions subjected to a gradient and skyrmions moving in a region irradiated with a single ion dose. In addition, the knowledge of the changes in diffusion induced by FIB allows to design a gradient that maximizes the asymmetry of the system.

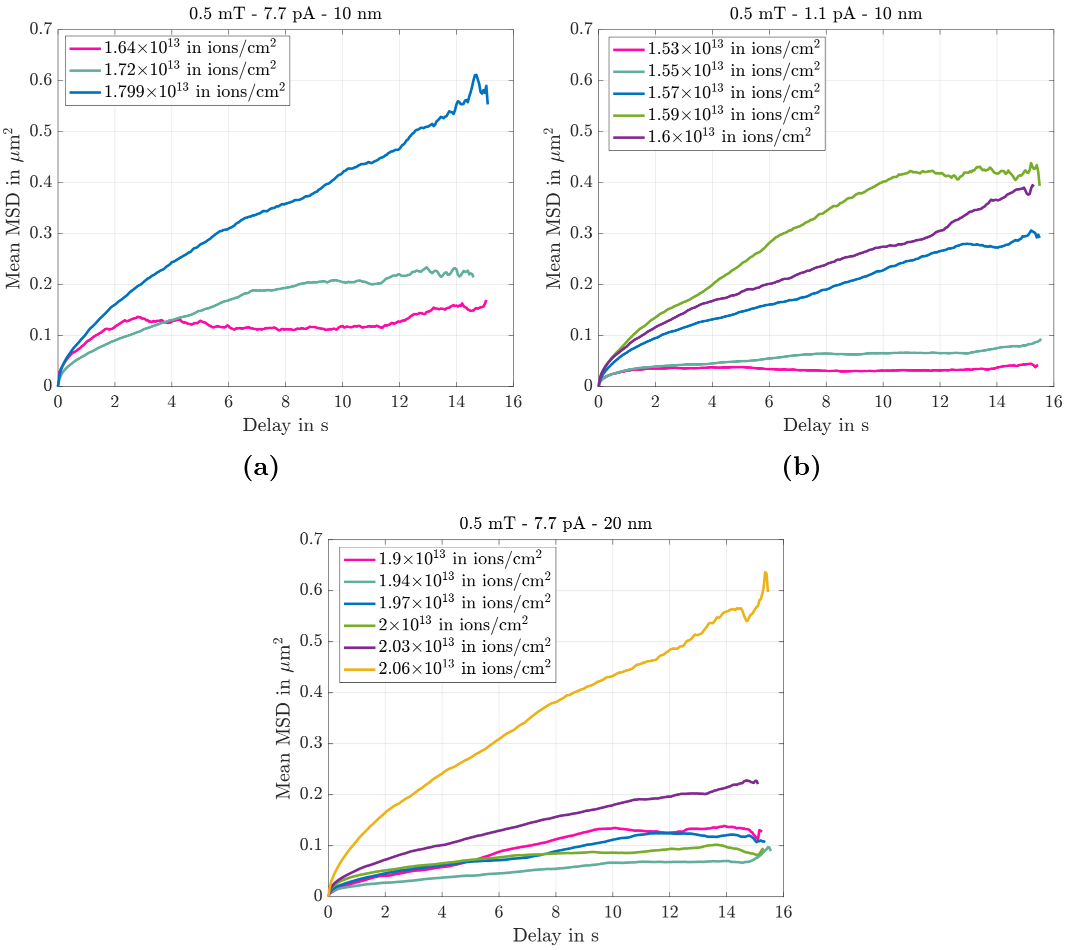

(a) **(b)** **(c)**

Figure 3.6: MSD curves at different ion doses and for 0.5 mT of field. Each plot has a different ion beam current and blur: a) 7.7 pA and 10 nm, b) 1.1 pA and 10 nm, and c) 7.7 pA and 20 nm. In each case, skyrmions are more diffusive when the higher ion doses are employed.

From Fig 3.6 we evince that skyrmions diffuse with Brownian motion and this behavior is accentuated with higher ion doses.

For the sake of completeness, we also retrieved the diffusion coefficient, which turned out to be on the same order of magnitude as the diffusivity calculated for skyrmions on the previous sample. The trend of increasing diffusivity with higher ion doses is clear in Fig 3.7.

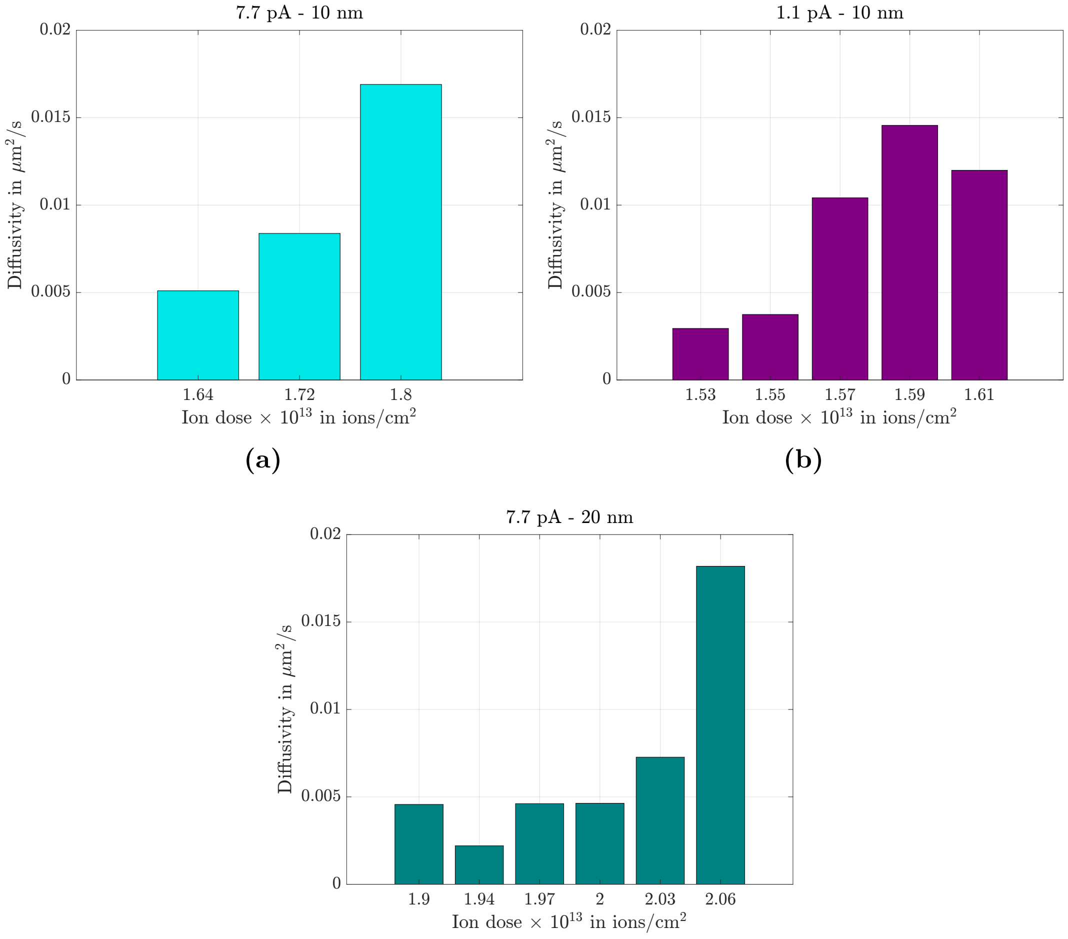

(a) **(b)**

(c)

Figure 3.7: Bar plot of the calculated diffusivities at 0.5 mT and with different ion doses, in each figure there is a combination of the ion beam current and blur: a) 7.7 pA and 10 nm, b) 1.1 pA and 10 nm, and c) 7.7 pA and 20 nm. Skyrmions' diffusivity is higher when the highest ion dose is employed.

Both combinations using 1.1 pA - 10 nm and 7.7 pA and 20 nm allow us to inspect skyrmions' behavior with at least five different ion doses, and each dose has a different effect on diffusion. Thus, gradients realized with these settings of the FIB, enable us to exploit these variations and possibly direct the diffusion of skyrmions.

3.4 Gradient of ion doses

The first attempt to realize a gradient of ion doses was with the irradiation of 10 rectangles with dimensions $8 \times 80\,\mu m^2$ inside a square of $80 \times 80\,\mu m^2$. Each rectangle has a different dose, chosen thanks to the previous analysis on the variation of diffusion. We quickly understood that patterning rectangles next to each other means that the contours of the rectangle are patterned and this impedes skyrmion diffusion between regions with different ion doses. With higher magnetic fields (Fig 3.8d), most of the outlines disappear but at the same time also skyrmions with more mobility annihilate. Furthermore, at high fields only pinned skyrmions remain and their motion is confined; thus the next gradients are patterned using another method. The best way to achieve a smoother change of ion doses with FIB is patterning through bitmaps, which are grayscale image files that allow precise control of dwell times and beam movements.

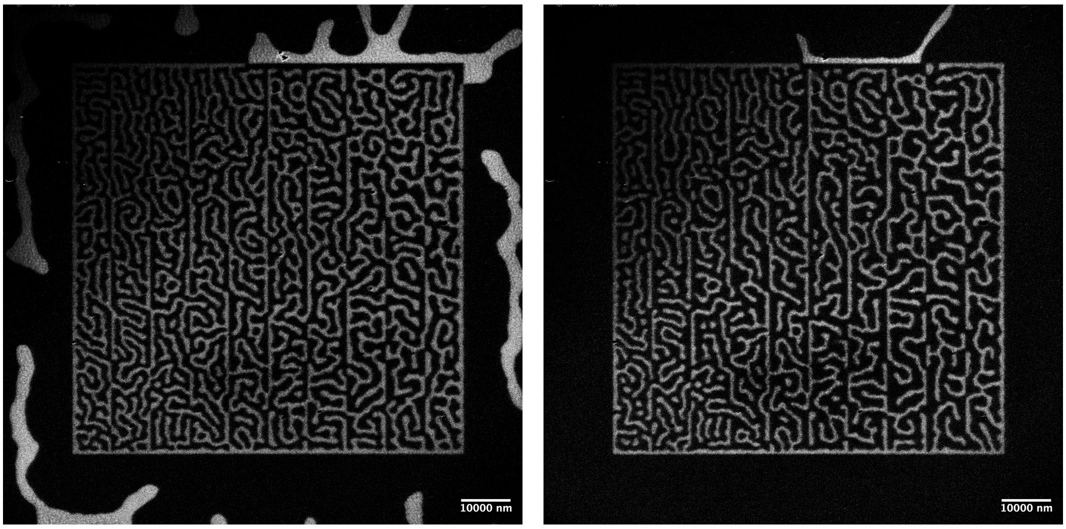

(a) 0.2 mT **(b)** 0.4 mT

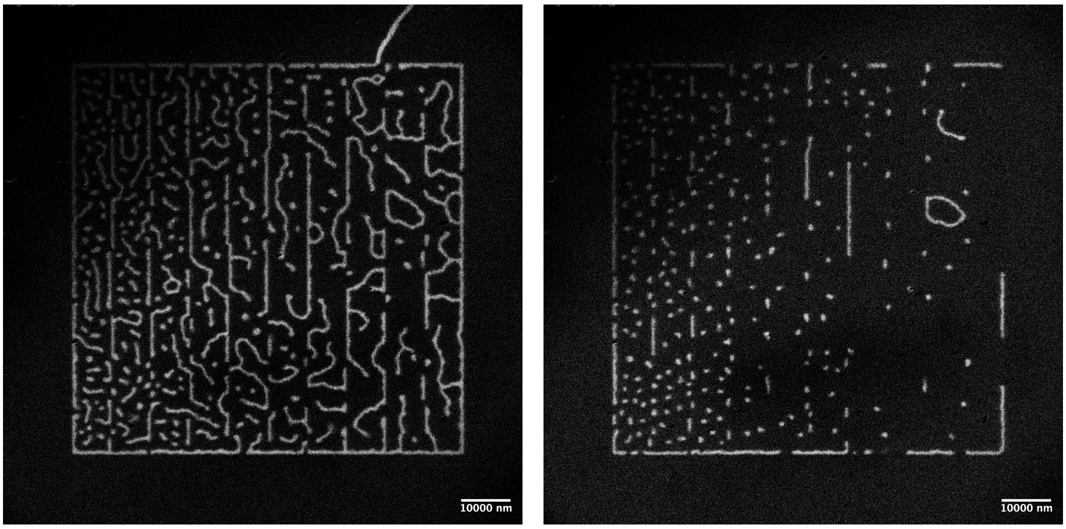

(c) 0.6 mT **(d)** 0.8 mT

Figure 3.8: WMOKE images of irradiated gradients on $W_{(3)}$/$CoFeB_{(1)}$/$MgO_{(1)}$/$Ta_{(3)}$ magnetic stack. The gradient is realized patterning narrow rectangles next to each other with ion doses ranging from $8.5 \times 10^{12}\, ions/cm^2$ to $7.5 \times 10^{13}\, ions/cm^2$, with 1.1 pA of ion beam current and 10 nm of blur.

3.4.1 Irradiation with bitmaps

The 24-bit bitmap files are created normalizing to a color value the dwell time for each pixel of the ion beam location.

- The red component does not control anything in this case, and is set equal to the blue component.

- The green component determines if the beam is blanked. Any value other than zero unblanks the beam.
- The blue component determines the dwell time per pixel. If the value is zero, the pixel is skipped. If the value is 1, the dwell time of a pixel is the lowest, while if the value is 255, the user-defined maximum value of dwell time is used.

The dwell time corresponding to the grayscale value is linearly interpolated on the basis of the value between 0 and the maximum dwell time. An example of a bitmap created for patterning gradients is given in Fig 3.9.

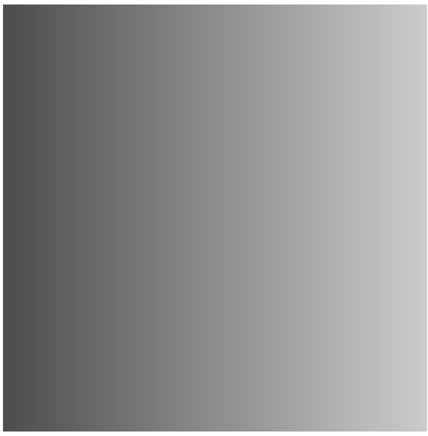

Figure 3.9: Example of a 24-bit bitmap file employed to pattern a gradient of ion doses. The gradient is visualized in grayscale, and the lightest part of the image corresponds to the highest dose, on the contrary the darkest part corresponds to the lowest dose.

Patterning with bitmaps allows pixel by pixel control, enabling the complete control of the ion beam movement and of the dwell time. Other than the dwell time, in a bitmap also the pixel density has to be carefully chosen. From the latter derives the scan pitch, which is the distance between two sequential beam positions, and the overlap between two beams, which is the ratio between the scan pitch and the ion beam diameter. Pixel spacing should be small enough to allow proper overlapping between the adjacent pixels so that a smooth and uniform profile can be fabricated. While we already discussed both the ion beam current and the blur that affect the ion beam diameter, now we report in Fig 3.10 the dimensions of the pattern and the pixel density.

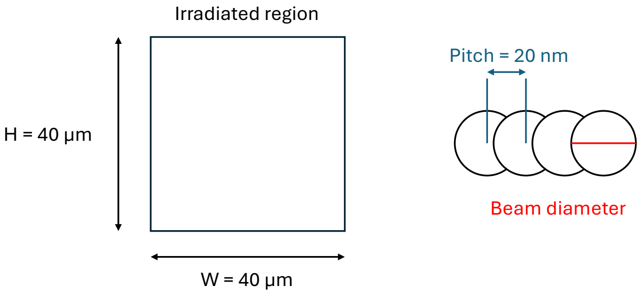

Figure 3.10: Illustration of the dimensions of the pattern of the bitmap and scan pitch. The size of the bitmap M × N is defined as: M = W/pitch and N = H/pitch, thus the pixel density is 2000 × 2000.

Before figuring out how to set the pitch of the bitmap, we tried with lower pixel densities. In Fig 3.11 there is the result of the bitmap patterning with a density of 100 × 100 pixels, the irradiation is not uniform and the desired ion dose is not achieved; however, there it is clear the "rastering" movement operated by the FIB during the patterning. The pixels of the bitmap image are scanned horizontally, line by line.

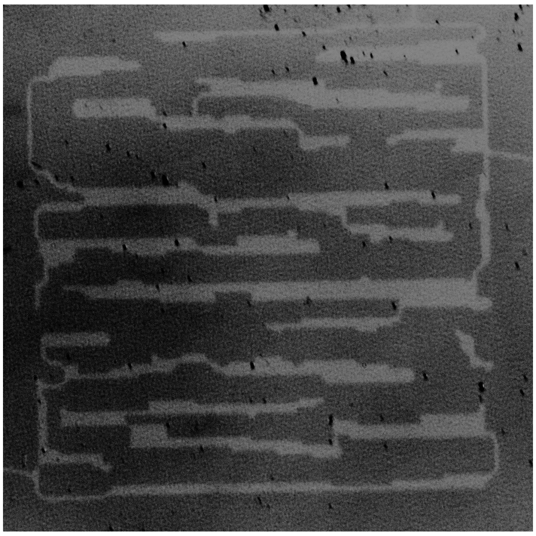

Figure 3.11: WMOKE image of a 40 × 40 μm^2 square irradiated using a bitmap with a density of 100 × 100 pixels.

Once we figured out how to successfully irradiate with bitmaps, and which is the best pixel density to employ, we got the first results of gradients.

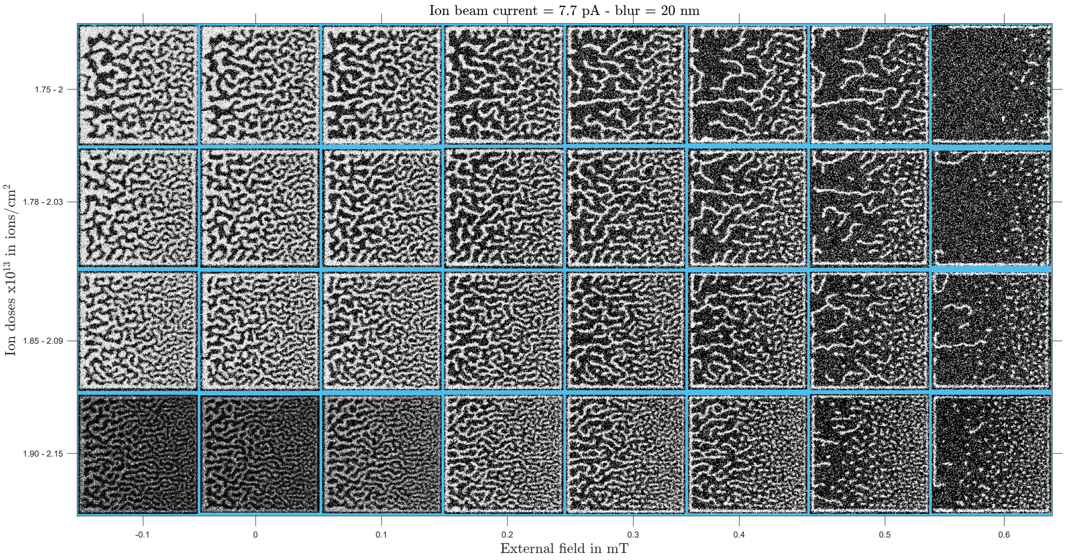

Figure 3.12: Evolution with respect to the applied magnetic field of domains and skyrmions in ion dose gradients realized with bitmaps in a $40 \times 40\,\mu m^2$ region. Each row has a different gradient of ion doses, starting from the top row towards the bottom row, the first gradient is from $1.75 \times 10^{13}\,\text{ions/cm}^2$ to $2.0 \times 10^{13}\,\text{ions/cm}^2$, then the second from $1.78 \times 10^{13}\,\text{ions/cm}^2$ to $2.03 \times 10^{13}\,\text{ions/cm}^2$, the third from $1.85 \times 10^{13}\,\text{ions/cm}^2$ to $2.09 \times 10^{13}\,\text{ions/cm}^2$, and the last gradient is from $1.90 \times 10^{13}\,\text{ions/cm}^2$ to $2.15 \times 10^{13}\,\text{ions/cm}^2$.

The first observation on the WMOKE images of Fig 3.12, is the change in size of domains within the same irradiated square, this proves the effect of different ion doses acting on the same square and the smooth irradiation profile achievable with bitmaps. In the regions with higher doses, domains are smaller and rip apart into skyrmions at lower magnetic fields as we expected. However, the goal was to observe a change in the diffusion of skyrmions, and in this case is neither possible to appreciate from the microscope nor to quantify. Skyrmions are present especially in the higher dose regions, and there their high density impedes the diffusion of skyrmions nucleated at lower doses towards the end of the gradient. To overcome this obstacle, we propose an alternative design of the gradient; instead of irradiating gradients in squares, we irradiate them in rectangular regions to force skyrmion motion along the same direction as the gradient and to better control the density of skyrmions. The idea is that adding confinement to the gradient it could be possible to guide their diffusive motion. Before proceeding with the irradiation of gradient stripes, we must study the effect of geometrical confinement alone on skyrmion diffusivity when irradiating rectangles instead of squares.

3.4.2 Skyrmion diffusion in confined geometries

The confinement analysis is carried out on rectangles of three different dimensions: $8 \times 40\,\mu m^2$, $10 \times 40\,\mu m^2$, and $20 \times 40\,\mu m^2$, as shown in Fig. 3.13.

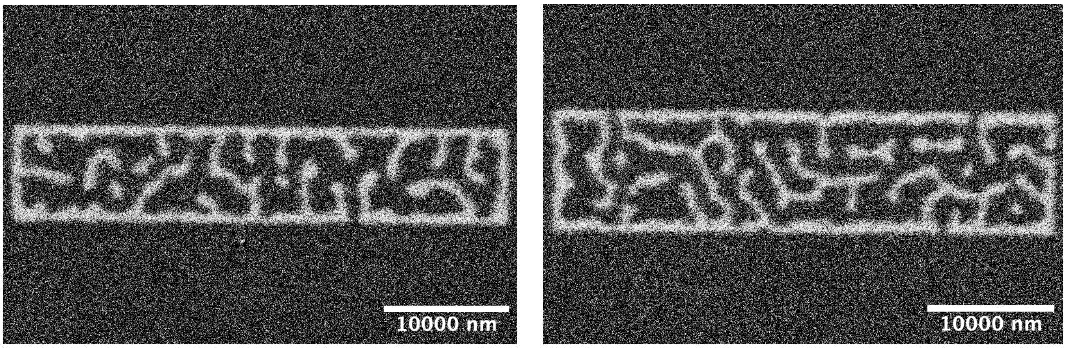

(a) $8 \times 40\,\mu m^2$ **(b)** $10 \times 40\,\mu m^2$

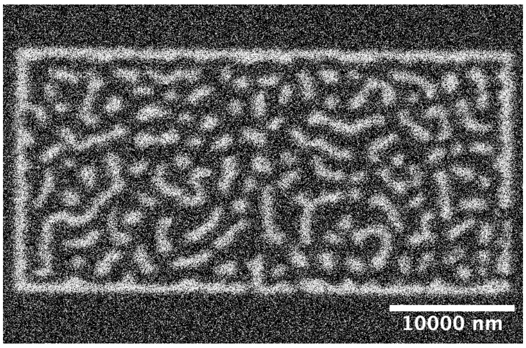

(c) $20 \times 40\,\mu m^2$

Figure 3.13: WMOKE images of irradiated rectangles, realized with 7.7 pA of beam current and 20 nm of blur. The images are taken at 0.6 mT, and the ion dose is $2.02 \times 10^{13}\,ions/cm^2$.

To explore the effects of the edge repulsions on the diffusion, we recorded the skyrmion motion and used the MSDanalyzer to analyze it. Again, through the MSD plots, we can identify which geometry does not impede diffusion when the MSD line has a linear time dependence.

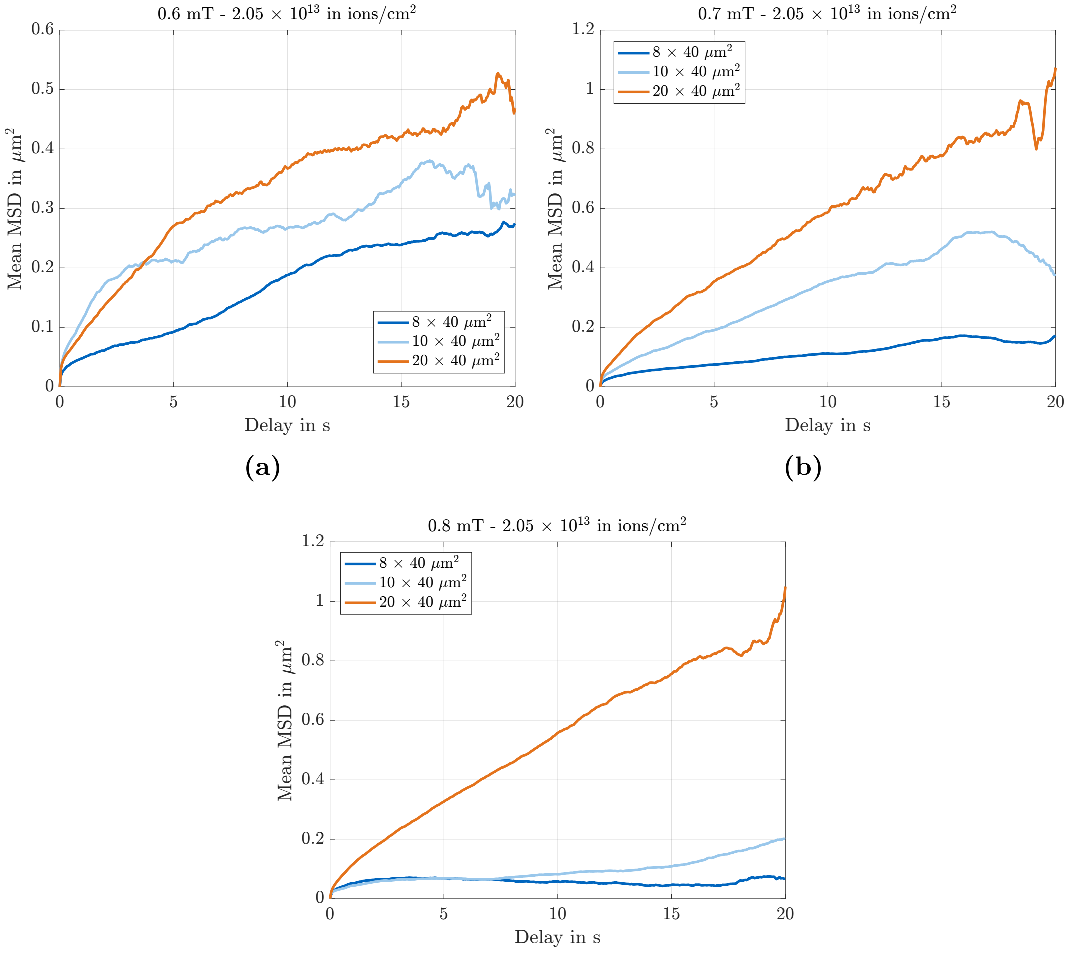

(a) **(b)**

(c)

Figure 3.14: MSD curves of skyrmions in rectangles with different aspect ratios at different fields. a) 0.6 mT, b) 0.7 mT and c) 0.8 mT. The ion dose for this comparison is the same for all the plots, it is 2.05×10^{13} ions/cm^2. In a), the blue curve for the $8 \times 40\,\mu m^2$ is less steep than the others, and using higher magnetic fields in b) and c), it approaches a plateau, reflecting the effect of geometry on skyrmions' confinement.

The plots of Figs 3.14a–3.14b, show that for $8 \times 40\,\mu m^2$ structures skyrmions are confined, while in the $10 \times 40\,\mu m^2$ case they are more diffusive. While for the same geometries, the analysis at 0.8 mT (Fig 3.14c) points out that at this field, not only are the remaining skyrmions pinned, but there is a strong effect from the edges of the rectangle that untimely stops skyrmion diffusion. The study of the interplay between the total number of skyrmions and the structure geometry that influences skyrmion diffusion was conducted by [36]. They proved that when skyrmions saturate all the available area, they create a more stable structure because skyrmions can no longer fluctuate between empty positions. While for the $10 \times 40\,\mu m^2$ rectangles, skyrmions have enough space to cover larger distances, indeed, the MSD does not reach a plateau value (for short delays).

Another indication that in $8 \times 40\,\mu m^2$ skyrmions are confined by the geometry comes from the evaluation of the diffusion coefficient (Fig 3.15).

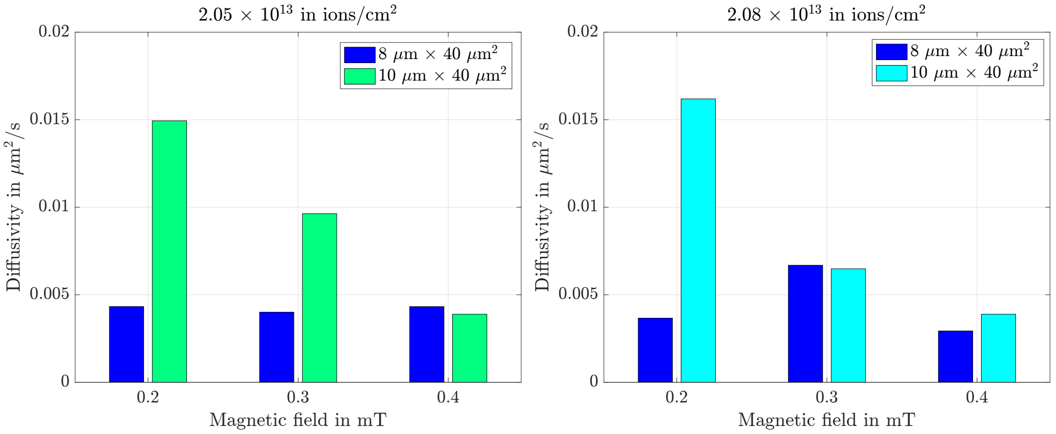

Figure 3.15: Diffusivity bar plot for skyrmions confined in rectangles with two different dimensions: $10 \times 40\,\mu m^2$ and $8 \times 40\,\mu m^2$.

With both ion doses, skyrmions in the $10 \times 40\,\mu m^2$ rectangles exhibit diffusivities with the same trend observed before. At lower magnetic fields, they diffuse more and D is higher, while for higher fields they are pinned, returning a lower D. On the other hand, in $8 \times 40\,\mu m^2$ skyrmions have a diffusion constant that doesn't change with the applied magnetic field or with the ion dose, confirming that the geometrical effects are dominating.
From the observation with the microscope, skyrmions in the $20 \times 40\,\mu m^2$ case are moving with Brownian motion, similarly to skyrmions in squares. Moreover, this aspect ratio is not enough to induce any restriction on the direction of motion. Thus, rectangles of $10 \times 40\,\mu m^2$ are chosen as the geometry for gradients.

3.4.3 Stripe gradients

The gradients are irradiated through bitmaps. On the sample, we patterned 20 bitmaps and in each bitmap there are three gradients whose shape is a stripe of $10 \times 40\,\mu m^2$, as it is visualized in Fig 3.16.

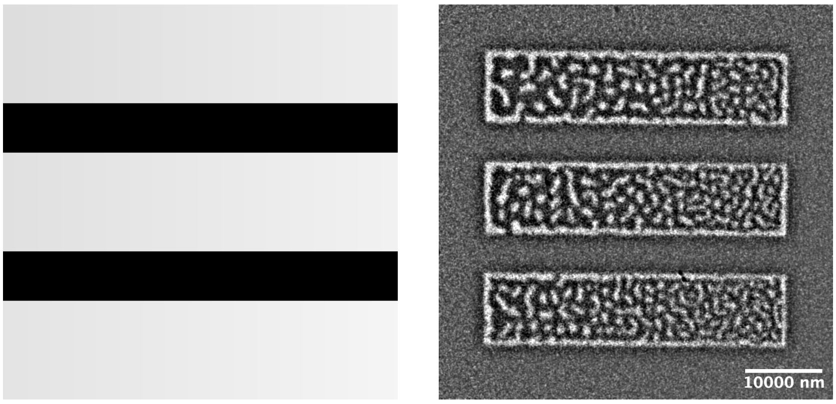

Figure 3.16: On the left, there is the bitmap realized to pattern three stripes with dimensions $10 \times 40\,\mu m^2$, and on the right the WMOKE image capturing the result of this irradiation.

Each gradient has a different range of ion doses, chosen on the basis of the previous analysis. For some ion dose ranges, skyrmions are mixed with domains, and even though we noticed high mobility of skyrmions, the presence of domains compromises the tracking, because the DoG algorithm is not suited for distinguishing skyrmions from domains. An example of such situations is in Fig 3.17, of these gradients, only the one at the bottom is successfully analyzed with TrackMate, its ion dose range is from 1.87×10^{13} ions/cm^2 to 2.02×10^{13} ions/cm^2.

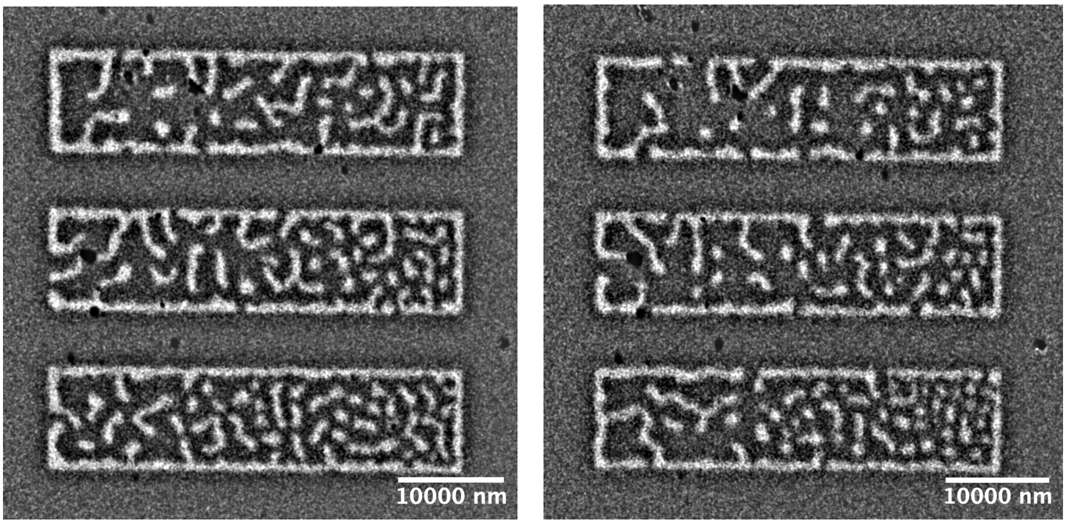

(a) 0.6 mT **(b)** 0.7 mT

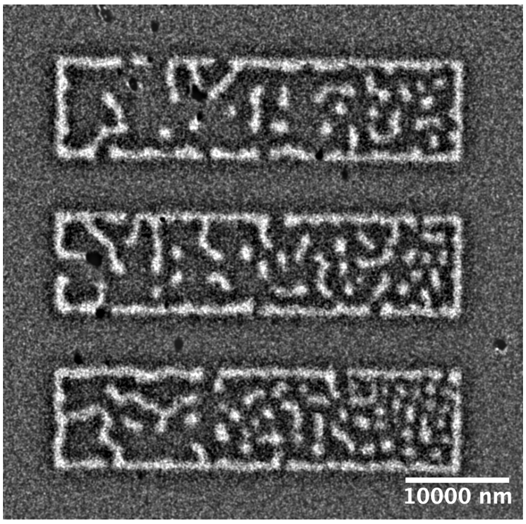

(c) 0.8 mT

Figure 3.17: WMOKE images of three gradients in rectangular shape, each subjected to different magnetic fields.

Six ion dose gradients produce interesting results; of these, three have a larger dose range, whereas the other three have been created with smaller dose differences. We first show the results of gradients with the smaller dose difference and for each gradient, we compared it with the result of the highest dose present in the gradient. The choice of this comparison comes from the observed trend of better diffusivity at higher ion doses, so it is done to find out if the gradient engineering allows skyrmions to acquire more mobility.

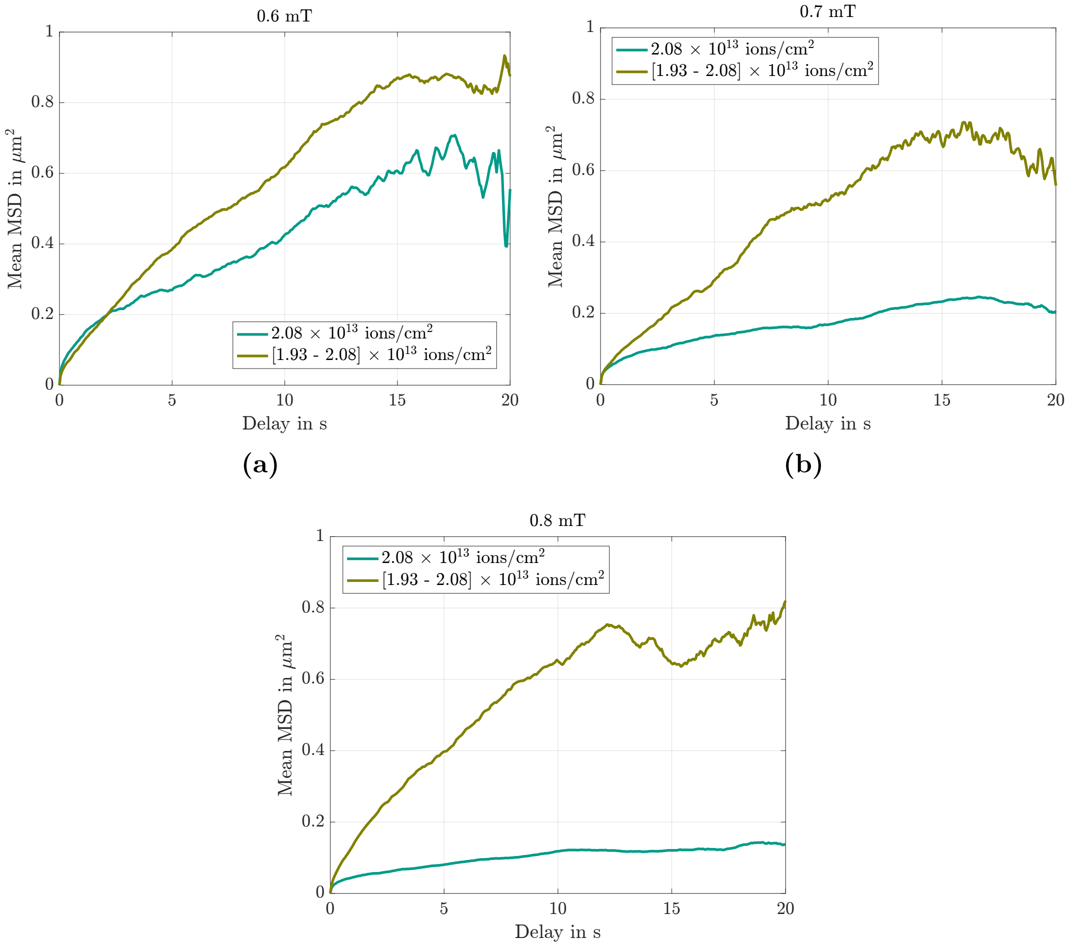

(a) **(b)**

(c)

Figure 3.18: MSD curves obtained with skyrmions moving in a gradient that ranges from $1.93 \times 10^{13}\,\text{ions/cm}^2$ to $2.08 \times 10^{13}\,\text{ions/cm}^2$, compared to the MSD curve of skyrmions at the highest ion dose ($2.08 \times 10^{13}\,\text{ions/cm}^2$), each at a different magnetic field.

In the comparisons of Fig 3.18, it is clear that in the gradient skyrmions have more mobility; indeed, their MSD curve is more linear than the one using only one ion dose. The other striking feature of employing the gradient together with the stripe geometry is that increasing the magnetic field, the behavior remains diffusive, instead of switching to confined. The same trend is observed for the other two gradients: one from $1.87 \times 10^{13}\,\text{ions/cm}^2$ to $2.02 \times 10^{13}\,\text{ions/cm}^2$ and the other from $1.90 \times 10^{13}\,\text{ions/cm}^2$ to $2.05 \times 10^{13}\,\text{ions/cm}^2$.

Passing to the other three gradients, with a larger difference of ion dose between the minimum and the maximum in the gradient, we expect different results, because in the same stripe, thus in less space, skyrmions experience more variations of ion doses.

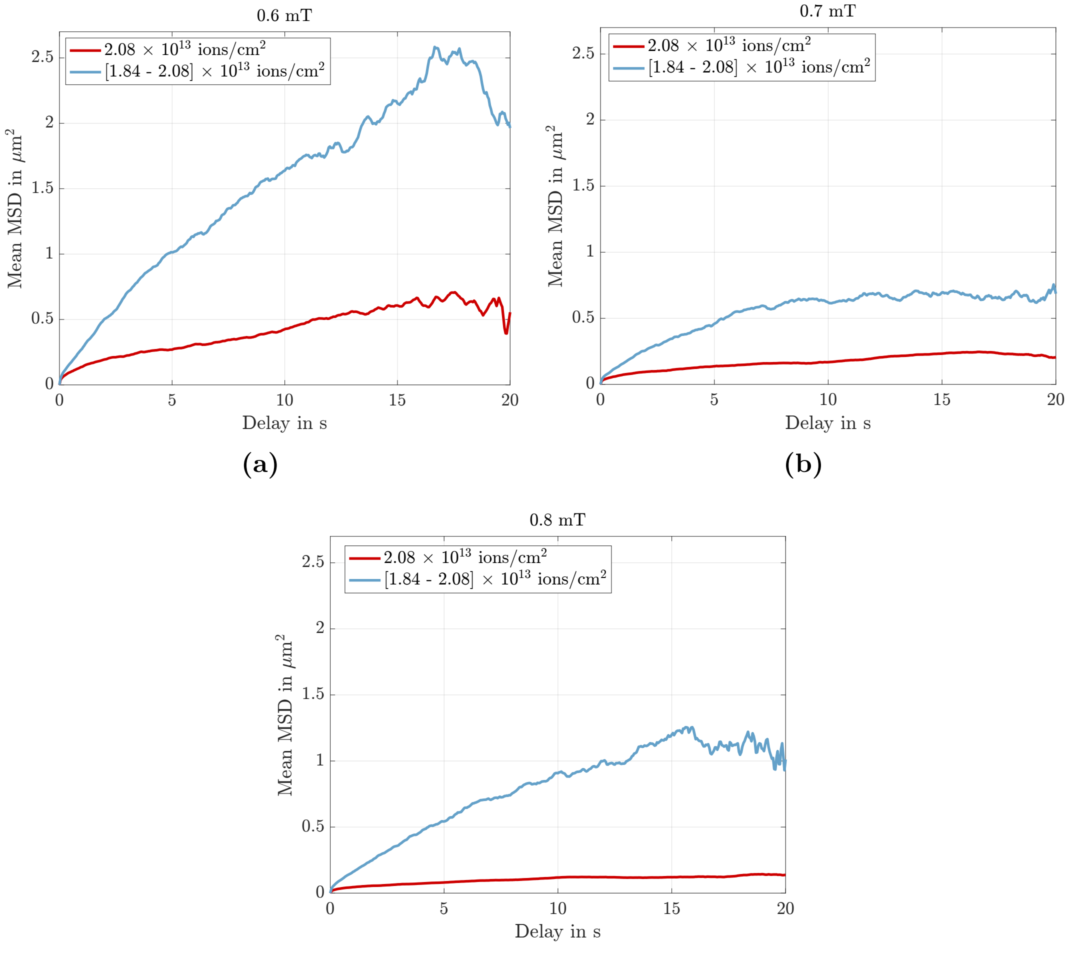

(a) (b)

(c)

Figure 3.19: MSD curves obtained with skyrmions moving in a gradient that ranges from 1.84×10^{13} ions/cm^2 to 2.08×10^{13} ions/cm^2, compared to the MSD curve of skyrmions at the highest ion dose (2.08×10^{13} ions/cm^2), each at a different magnetic field.

Before (Fig 3.18), the gradient showed better results than a single ion dose with a big margin; whereas, in Fig 3.19b skyrmions motion seems confined. Actually, looking at the results, each in its own scale, in the gradients skyrmions motion is never restricted; it is the very large distances covered by skyrmions in the case of Fig 3.19a to make the other curves look confined. The greater diffusion experienced in the gradient is retrieved also for the other two gradients, one from 1.78×10^{13} ions/cm^2 to 2.02×10^{13} ions/cm^2 and the other from 1.81×10^{13} ions/cm^2 to 2.05×10^{13} ions/cm^2.

To have a direct comparison between which gradient, with lower or higher differences of doses, has a better impact on diffusion, we examined the diffusivity.

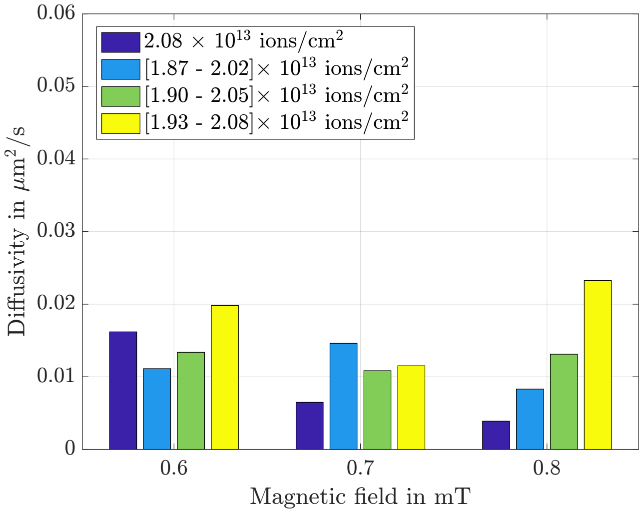

(a)

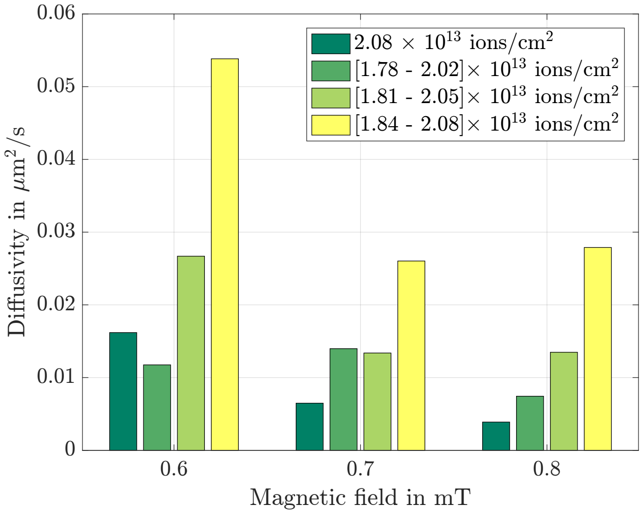

(b)

Figure 3.20: Bar plots of the diffusivity, (a) of gradients with lower ion dose difference, and (b) of gradients with higher ion dose difference.

It is undoubtedly the gradient 1.84×10^{13} ions/cm^2 to 2.08×10^{13} ions/cm^2 shows the best diffusivity, and it is not only greater than the one of skyrmions in a $10\times40\,\mu m^2$ rectangle at $2.08\times10^{13}\, ions/cm^2$, but it is even higher than the diffusivity of skyrmions in $80\times80\,\mu m^2$ squares. This shows the improvement of the Brownian motion achieved by both the geometrical confinement and ion dose gradient.

3.5 Conclusions

The research illustrated in this chapter was stimulated by the need to exploit the "richness" of Brownian motion. From the example of other computing schemes, all started with the study of biological functions that take advantage of fluctuations. The evinced principle is that to process the information associated with a physical entity, in our case the magnetic skyrmion, and using Brownian motion for doing so, the latter must be modulated.

Therefore, the idea is to realize a gradient of ion doses that could affect the diffusion of skyrmions and direct them along the direction of the gradient.

FIB is a very powerful tool to tune the ion density, and the best way to obtain the gradient is to construct a bitmap of dwell time and pattern with it. We conducted a detailed analysis of the FIB settings needed for the bitmap, the ion beam current, the defocus diameter, and the pixel density. This work could be significant because it can be integrated as the fabrication process in neuromorphic devices, such as for [37, 38]. In those artificial neurons, the domain wall motion along a gradient of anisotropy is exploited to reproduce the leaking feature of neurons. By knowing the variation in anisotropy related to ion doses, it can be created with FIB. Another aspect to consider when using FIB is its compatibility with other CMOS technologies. With the high demand of new devices, and thus of new expensive fabrication techniques, it is valuable when a new technology opens up to new applications using the same processes as the previous one. Completely changing all devices to spintronic devices is very ambitious, while incorporating this technology with CMOS is more utilizable in the near future.

This idea is validated by another biological example. Indeed, our brain is a highly heterogeneous architecture, with specific functions being conducted in different areas by different cells. The diversity in the components allows a reduction of the computational cost [39]. On the other hand, von Neumann architecture, the dominant computational model, uses small number of powerful computational units that take in a lot of data. By analogy to the brain, exploiting heterogeneous devices that are very specific and highly efficient, like magnetic devices together with scaled CMOS devices, may be one possibility to answer the demand for new processing units.

Going back to the main topic, to achieve the goal of directing diffusion of skyrmions, the gradient of ion doses alone is proved not to be enough. The strategy became to change the shape of the irradiated structure in which there is a gradient. From a square, we passed to a rectangle to guide the Brownian motion through a gradient and through confinement. This opened the necessity to analyze first the confinement effects on Brownian motion. We found the aspect ratio of the rectangle for which the patterned edges don't impede the skyrmion diffusion.

In the end, the combined effect of ion dose gradient and confinement led to an increase in diffusion, but not to directed motion. The expected behavior was for skyrmions to move from regions of high anisotropy (low ion dose) to regions of low anisotropy (high ion dose), because this is more energetically favorable. However, the main

limitation to the development of this idea is that skyrmions at the beginning of the gradient don't have enough space to move towards the other end, since it is occupied by skyrmions nucleated at higher doses. Effectively tuning skyrmion density in the gradient would be the next step to complete this analysis.
Eventually, skyrmions may be moved by current pulses and achieve directionality, while the modulation of the diffusion through the gradient may serve as the leaking mechanism for an artificial neuron. Or the rectangular gradient could be the chamber where skyrmions diffuse in a reshuffler device, as the one proposed in [12]. Furthermore, the precise control of movements and dwell times achievable while patterning with bitmaps unlocks the possibility of creating more intricate patterns of ion doses and thus of anisotropy, or, as suggested in this thesis, different diffusivities. An idea could be to put near each other gradients with diverse variations of ion doses and different directions, forcing skyrmion motion to happen in "bursts" (Fig 3.21).

Figure 3.21: 24-bit bitmap pattern for skyrmion "burst" motion. Darker areas correspond to smaller dwell times and light areas to longer dwell times.

All in all, the engineering of the gradient produces a controlled diffusion of skyrmions and highlights how versatile the modulation of skyrmion properties through ion irradiation is.

Appendix A

Experimental set-up

In this section, the instrument used to pattern the thin films, the Focused Ion Beam (FIB), is illustrated. The patterning specifics, like the ion beam current and beams overlap, and the realization of bitmaps are discussed in chapter 3. Then there is an overview of the wide-field magneto optical microscopy (WMOKE) used to obtain images for magnetic domains and skyrmions analysis.

A.1 Focused Ion Beam

Focused ion beam technology was developed as a result of research on the liquid-metal ion sources (LMIS). Since its commercialization, it has been widely used for nano-fabrication purposes, because it has four functionalities: milling, deposition, implantation and imaging. The instrument that we have been using is a DualBeam system, thus it incorporates both a FIB and a SEM (Scanning Electron Microscope). In this way, it achieves tasks beyond the limitations of both systems. Indeed, the electron beam is not suited for lithographic purposes; it has a slower deposition rate and difficulties penetrating harder materials without suffering distortion effects due to local charge build-up. The reason for these disadvantages arises from the electrons' low mass. Therefore, using an ion beam has all the advantages coming from more massive elements. When the FIB directs a stream of high-energy ionized atoms towards a surface, ions collide with the atoms of the sample, and if the collisions are elastic, the obtained effect is sputtering. The capabilities of removing atoms for milling or deposition with high resolution, or implantation, are the mainly used features of FIB. Aa a matter of fact for the study of this thesis, implanting ions in the magnetic stack offers the possibility to tune the properties of the stack.

Moreover, if ions have inelastic collisions with the surface's atoms, secondary electrons are produced and these are exploited for imaging purposes. This implies that during milling, secondary electrons allow imaging. However, this FIB can cause undesired damage to the sample, especially considering that ions are larger and while penetrating the surface, their size causes more interactions, breaking of bonds and even changes in the chemical state of the material [40].

In a DualBeam system, imaging can be done with the electron beam, limiting the ion beam use to lithography and not damaging the sample. At the top of the ion beam column there is the LMIS that produces Ga ions, then the ions are pulled out and focused. Both the columns for ions and electrons are based on the same principle, as it is shown in Fig A.1, the stream of charged particles is focused by a series of lenses and apertures. Anyway, the control mechanisms between the two beams are different, given that ions are more massive and usually positively charged, while electrons are always negatively charged. The higher kinetic energy of ions requires greater fields to be focused than electrons. Electron and ion optics employ magnetic and electric fields to change the particles' path, and ion lenses are exclusively electrostatic lenses.

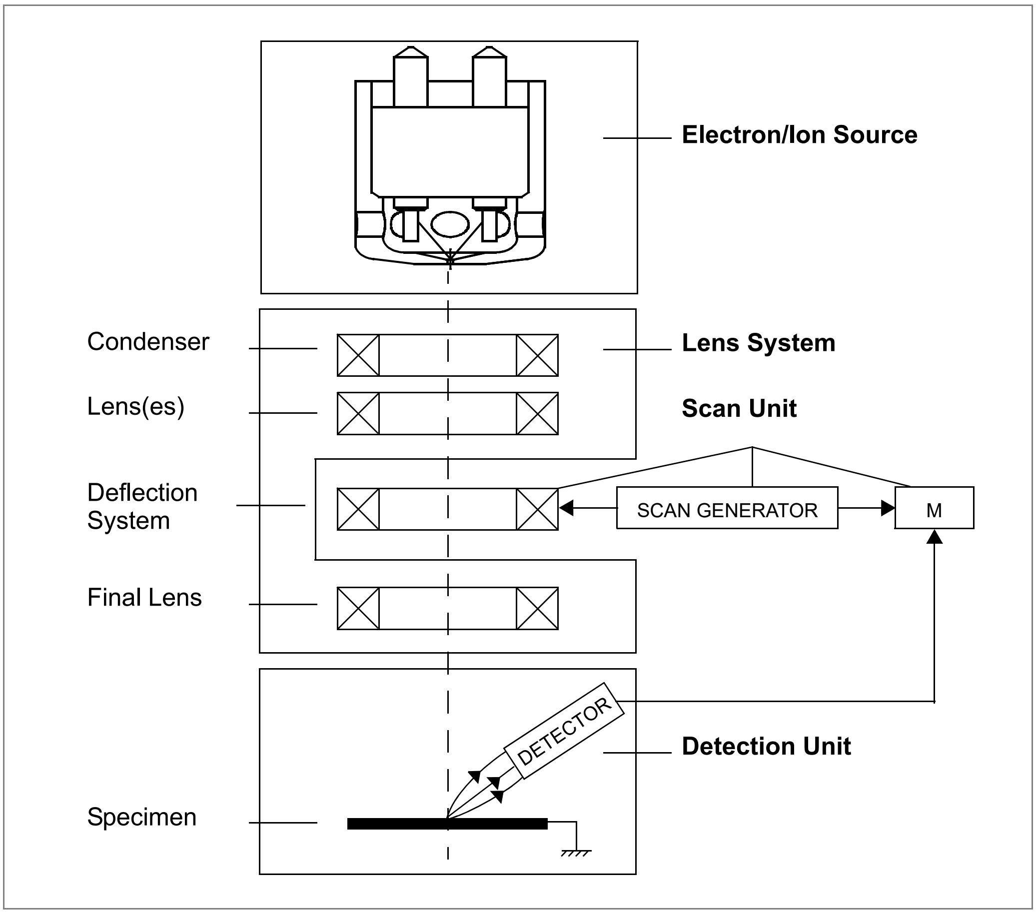

Figure A.1: Column schematic overview present on the user operational manual of the Helios 5 DualBeam system.

A.2 Magneto-optical microscopy

Magneto-optical effects arise from the interaction of electromagnetic waves and magnetized materials. The magneto-optical Kerr effect is based on the rotation of the plane of polarization of light during reflection from a magnetized surface. In this way, the state of magnetization is detected and used to create the magnetic image. Three different types of MOKE can be distinguished, which depend on the orientation of the magnetization relative to the plane of incidence and the orientation of the polarization of light. The configurations are illustrated in Fig A.2.

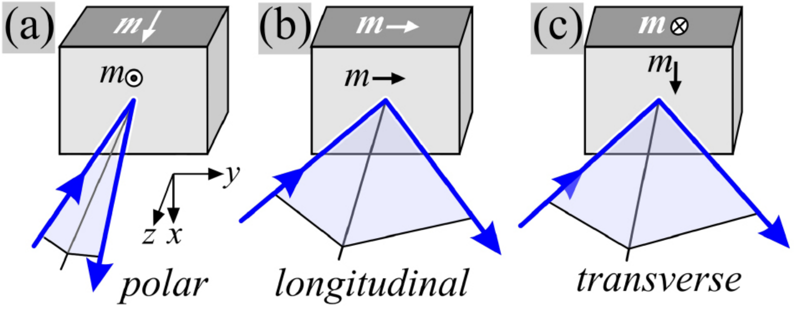

Figure A.2: The three basic configurations of the (a) polar, (b) longitudinal, and (c) transverse magneto-optical Kerr effect. The unit vector of magnetization m lies along the easy axis [41].

For this thesis, the imaging of magnetic domains and skyrmions is performed through the WMOKE microscope. The wide-field MOKE microscope employs an LED to illuminate a wide area of the sample and an analyzer to detect the reflected light, which allows fast imaging of magnetic textures.

Bibliography

[1] Sai Li, Wang Kang, Xichao Zhang, Tianxiao Nie, Yan Zhou, Kang L. Wang, and Weisheng Zhao. “Magnetic skyrmions for unconventional computing”. In: *Mater. Horiz.* 8.3 (2021), pp. 854–868.

[2] Albert Fert, Vincent Cros, and Joao Sampaio. “Skyrmions on the track”. In: *Nature Nanotechnology* 8.3 (2013), pp. 152–156.

[3] A. P. Guimarães. *Principles of Nanomagnetism*. NanoScience and Technology. Berlin, Heidelberg: Springer, 2009. ISBN: 978-3-642-26111-4. URL: `https://link.springer.com/book/10.1007/978-3-642-01482-6`.

[4] Karin Everschor-Sitte and Matthias Sitte. “Real-space Berry phases: Skyrmion soccer (invited)”. In: *Journal of Applied Physics* 115.17 (2014), p. 172602.

[5] Xichao Zhang et al. “Skyrmion-electronics: writing, deleting, reading and processing magnetic skyrmions toward spintronic applications”. In: *Journal of Physics: Condensed Matter* 32.14 (2020), p. 143001.

[6] Chung-Soo Kim, Sung-Hoon Ahn, and Dong-Young Jang. “Developments in micro/nanoscale fabrication by focused ion beams”. In: *Vacuum* 86.8 (2012), pp. 1014–1035.

[7] Roméo Juge et al. “Helium Ions Put Magnetic Skyrmions on the Track”. In: *Nano Letters* 21.7 (2021), pp. 2989–2996.

[8] Simon Mendisch, Fabrizio Riente, Valentin Ahrens, Luca Gnoli, Michael Haider, Matthias Opel, Martina Kiechle, Massimo Ruo Roch, and Markus Becherer. “Controlling Domain-Wall Nucleation in Ta/Co-Fe-B/MgO Nanomagnets via Local Ga^+ Ion Irradiation”. In: *Phys. Rev. Appl.* 16 (2021), p. 014039.

[9] Valentin Ahrens, Clara Kiesselbach, Luca Gnoli, Domenico Giuliano, Simon Mendisch, Martina Kiechle, Fabrizio Riente, and Markus Becherer. “Skyrmions Under Control—FIB Irradiation as a Versatile Tool for Skyrmion Circuits”. In: *Advanced Materials* 35.2 (2023), p. 2207321.

[10] Yue Hu et al. “Precise Tuning of Skyrmion Density in a Controllable Manner by Ion Irradiation”. In: *ACS Applied Materials & Interfaces* 14.29 (2022), pp. 34011–34019.

[11] Valentin Ahrens, Luca Gnoli, Domenico Giuliano, Simon Mendisch, Martina Kiechle, Fabrizio Riente, and Markus Becherer. “Skyrmion velocities in FIB irradiated W/CoFeB/MgO thin films”. In: *AIP Advances* 12.3 (2022), p. 035325.

[12] Daniele Pinna, Flavio Abreu Araujo, J-V Kim, Vincent Cros, Damien Querlioz, Pierre Bessiere, Jacques Droulez, and Julie Grollier. “Skyrmion gas manipulation for probabilistic computing”. In: *Physical Review Applied* 9.6 (2018), p. 064018.

[13] Jakub Zázvorka et al. “Thermal skyrmion diffusion used in a reshuffler device”. In: *Nature nanotechnology* 14.7 (2019), pp. 658–661.

[14] Daniele Pinna, George Bourianoff, and Karin Everschor-Sitte. “Reservoir computing with random skyrmion textures”. In: *Physical Review Applied* 14.5 (2014), p. 054020.

[15] Klaus Raab, Maarten A Brems, Grischa Beneke, Takaaki Dohi, Jan Rothörl, Fabian Kammerbauer, Johan H Mentink, and Mathias Kläui. “Brownian reservoir computing realized using geometrically confined skyrmion dynamics”. In: *Nature Communications* 13.1 (2022), p. 6982.

[16] Michael J. Saxton. *Modeling 2D and 3D Diffusion.* Humana Press, 2007, pp. 295–321.

[17] Nadine Tarantino, Jean-Yves Tinevez, Elizabeth Faris Crowell, Bertrand Boisson, Ricardo Henriques, Musa Mhlanga, Fabrice Agou, Alain Israël, and Emmanuel Laplantine. “TNF and IL-1 exhibit distinct ubiquitin requirements for inducing NEMO–IKK supramolecular structures”. In: *Journal of Cell Biology* 204.2 (2014), pp. 231–245.

[18] Johannes Schindelin et al. “Fiji: an open-source platform for biological-image analysis”. In: *Nature methods* 9.7 (2012), pp. 676–682.

[19] Jean-Yves Tinevez, Nick Perry, Johannes Schindelin, Genevieve M Hoopes, Gregory D Reynolds, Emmanuel Laplantine, Sebastian Y Bednarek, Spencer L Shorte, and Kevin W Eliceiri. “TrackMate: An open and extensible platform for single-particle tracking”. In: *Methods* 115 (2017), pp. 80–90.

[20] Khuloud Jaqaman, Dinah Loerke, Marcel Mettlen, Hsuan Kuwata, Sergio Grinstein, Sandra L. Schmid, and Gaudenz Danuser. “Robust single-particle tracking in live-cell time-lapse sequences”. In: *Nature Methods* 5.8 (2008), pp. 695–702.

[21] Raphael Gruber et al. “Skyrmion pinning energetics in thin film systems”. In: *Nature Communications* 13.1 (2022), p. 3144.

[22] Imara Lima Fernandes, Juba Bouaziz, Stefan Blügel, and Samir Lounis. “Universality of defect-skyrmion interaction profiles”. In: *Nature communications* 9.1 (2018), p. 4395.

[23] Xiaoxuan Zhao et al. “Enhancing domain wall velocity through interface intermixing in W-CoFeB-MgO films with perpendicular anisotropy”. In: *Applied Physics Letters* 115.12 (2019).

[24] Erik Kalz, Hidde Derk Vuijk, Iman Abdoli, Jens-Uwe Sommer, Hartmut Löwen, and Abhinav Sharma. "Collisions enhance self-diffusion in odd-diffusive systems". In: *Physical Review Letters* 129.9 (2022), p. 090601.

[25] Michael J. Saxton. "Single-particle tracking: the distribution of diffusion coefficients". In: *Biophysical Journal* 72.4 (1997), pp. 1744–1753.

[26] Takayuki Nozaki, Yuma Jibiki, Minori Goto, Eiiti Tamura, Tomohiro Nozaki, Hitoshi Kubota, Akio Fukushima, Shinji Yuasa, and Yoshishige Suzuki. "Brownian motion of skyrmion bubbles and its control by voltage applications". In: *Applied Physics Letters* 114.1 (2019).

[27] Philipp Rieger, Markus Weißenhofer, and Ulrich Nowak. "Defect-enhanced diffusion of magnetic skyrmions". In: *Physical Review B* 108.14 (2023), p. 144417.

[28] Toshio Yanagida. "Fluctuation as a tool of biological molecular machines". In: *BioSystems* 93.1-2 (2008), pp. 3–7.

[29] Harley H McAdams and Adam Arkin. "It's a noisy business! Genetic regulation at the nanomolar scale". In: *Trends in genetics* 15.2 (1999), pp. 65–69.

[30] Srinandan Dasmahapatra, Joern Werner, and Klaus-Peter Zauner. "Noise as a computational resource". In: *International Journal of Unconventional Computing* 4 (2006), pp. 305–319.

[31] Peter Hänggi, Fabio Marchesoni, and Franco Nori. "Brownian motors". In: *Annalen der Physik* 517.1-3 (2005), pp. 51–70.

[32] Jeroen H Franken, Mark Hoeijmakers, Reinoud Lavrijsen, and Henk JM Swagten. "Domain-wall pinning by local control of anisotropy in Pt/Co/Pt strips". In: *Journal of Physics: Condensed Matter* 24.2 (2011), p. 024216.

[33] L Herrera Diez et al. "Enhancement of the Dzyaloshinskii-Moriya interaction and domain wall velocity through interface intermixing in Ta/CoFeB/MgO". In: *Physical Review B* 99.5 (2019), p. 054431.

[34] Ismael Ribeiro de Assis, Ingrid Mertig, and Börge Göbel. "Skyrmion motion in magnetic anisotropy gradients: Acceleration caused by deformation". In: *Physical Review B* 108.14 (2023), p. 144438.

[35] Nabil Bassim, Keana Scott, and Lucille A Giannuzzi. "Recent advances in focused ion beam technology and applications". In: *Mrs Bulletin* 39.4 (2014), pp. 317–325.

[36] Chengkun Song et al. "Commensurability between element symmetry and the number of skyrmions governing skyrmion diffusion in confined geometries". In: *Advanced Functional Materials* 31.19 (2021), p. 2010739.

[37] Enrico Gaggio, Mariagrazia Graziano, and Fabrizio Riente. "DMI Influence on the Integration, Leakage, and Threshold Property of Domain Wall Based Neurons". In: *IEEE Transactions on Electron Devices* 71.4 (2024), pp. 2696–2701.

[38] Wesley H Brigner, Xuan Hu, Naimul Hassan, Christopher H Bennett, Jean Anne C Incorvia, Felipe Garcia-Sanchez, and Joseph S Friedman. “Graded-anisotropy-induced magnetic domain wall drift for an artificial spintronic leaky integrate-and-fire neuron”. In: *IEEE Journal on Exploratory Solid-State Computational Devices and Circuits* 5.1 (2019), pp. 19–24.

[39] Vijay Balasubramanian. “Heterogeneity and efficiency in the brain”. In: *Proceedings of the IEEE* 103.8 (2015), pp. 1346–1358.

[40] Yao Nan. *Introduction to the focused ion beam system.* Cambridge University Press, 2007, pp. 1–30.

[41] Jeffrey McCord. “Progress in magnetic domain observation by advanced magneto-optical microscopy”. In: *Journal of Physics D: Applied Physics* 48.33 (2015), p. 333001.